



1    **New insight into the formation and aging processes of organic**  
2    **aerosol from positive matrix factorization (PMF) analysis of**  
3    **ambient FIGAERO-CIMS thermograms**

4    Mingfu Cai<sup>1,2,3</sup>, Bin Yuan<sup>2,3</sup>, Weiwei Hu<sup>4,5\*</sup>, Ye Chenshuo<sup>6</sup>, Shan Huang<sup>2,3</sup>, Suxia  
5    Yang<sup>7</sup>, Wei Chen<sup>4</sup>, Yuwen Peng<sup>2,3</sup>, Zhaoxiong Deng<sup>2,3</sup>, Jun Zhao<sup>8†</sup>, Duohong Chen<sup>9</sup>,  
6    Jiaren Sun<sup>1</sup>, Min Shao<sup>2,3</sup>

7    <sup>1</sup>Guangdong Province Engineering Laboratory for Air Pollution Control, Guangdong Provincial Key  
8    Laboratory of Water and Air Pollution Control, South China Institute of Environmental Sciences, MEE,  
9    Guangzhou 510655, China

10    <sup>2</sup>Institute for Environmental and Climate Research, Jinan University, Guangzhou 511443, China

11    <sup>3</sup>Guangdong-Hongkong-Macao Joint Laboratory of Collaborative Innovation for Environmental  
12    Quality, Jinan University, Guangzhou 510632, China

13    <sup>4</sup>State Key Laboratory of Advanced Environmental Technology, Guangzhou Institute of Geochemistry,  
14    Chinese Academy of Sciences, Guangzhou, 510640, China

15    <sup>5</sup>Guangdong-Hong Kong-Macao Joint Laboratory for Environmental Pollution and Control,  
16    Guangzhou Institute of Geochemistry, Chinese Academy of Science, Guangzhou, China

17    <sup>6</sup>Guangdong Provincial Academy of Environmental Science, Guangzhou, 510045, China

18    <sup>7</sup>Guangzhou Research Institute of Environment Protection Co.,Ltd, Guangzhou 510620, China

19    <sup>8</sup>School of Atmospheric Sciences, Guangdong Province Key Laboratory for Climate Change and  
20    Natural Disaster Studies, and Institute of Earth Climate and Environment System, Sun Yat-sen  
21    University, Zhuhai 519082, China

22    <sup>9</sup>Guangdong Environmental Monitoring Center, Guangzhou 510308, China

23    <sup>†</sup>Deceased, 10/2024

24

25    Correspondence to: Weiwei Hu (weiwei.hu@gig.ac.cn)

26



## Abstract

Secondary organic aerosol (SOA) is an important component of organic aerosol (OA), yet its atmospheric evolution and impacts on volatility remain poorly understood. In this study, we investigated the volatility of different types of SOA at a downwind site of the Pearl River Delta (PRD) region in the fall of 2019, using a time-of-flight chemical ionization mass spectrometer coupled with a Filter Inlet for Gases and Aerosol (FIGAERO-CIMS). Positive matrix factorization (PMF) analysis was performed on the thermogram data of organic compounds (referred as FIGAERO-OA) measured by the FIGAERO-CIMS. Eight factors were resolved, including six daytime chemistry related factors, a biomass burning related factor (BB-LVOA, 10% of the FIGAERO-OA), and a nighttime chemistry related factor (Night-LVOA, 15%) along with their corresponding volatility. Day-HNO<sub>x</sub>-LVOA (12%) and Day-LNO<sub>x</sub>-LVOA (11%) were mainly formed through gas-particle partitioning. Increasing NO<sub>x</sub> levels mainly affected SOA formation through gas-particle partitioning, suppressing the formation of low-volatile organic vapors, and thus promoting the formation of relatively high volatile OA with a higher N:C ratio. Two aged OA factors, Day-aged-LVOA (16%) and Day-aged-ELVOA (11%), were attributed to daytime photochemical aging of pre-existing OA. In addition, the daytime formation of Day-urban-LVOA (16%) and Day-urban-ELVOA (7%) could only be observed in the urban plume. Results show that both gas-particle partitioning (36%) and photochemical aging (30%) accounted for a major fraction in FIGAERO-OA in the afternoon during the urban air masses period, especially for high-NO<sub>x</sub>-like pathway (~21%). In general, the six daytime OA factors collectively explain the majority (82%) of daytime SOA identified by an aerosol mass spectrometer (AMS). While BB-LVOA and Night-LVOA accounted for 13% of biomass burning OA and 48% of nighttime chemistry OA observed by AMS, respectively. Our PMF analysis also demonstrated that the highly oxygenated OA and hydrocarbon-like OA cannot be identified with FIGAERO-CIMS in this study. In summary, our results show that the volatility of OA is strongly governed by its formation pathways and subsequent atmospheric aging processes.



## 54 1. Introduction

55 Secondary organic aerosols (SOA), a major component of fine particulate matter (PM<sub>2.5</sub>) in  
56 China (Zhou et al., 2020), exert profound influences on climate change, human health, and air  
57 quality (Arias et al., 2021; Apte et al., 2018; Huang et al., 2014). Despite notable reductions in  
58 primary emission in recent years, SOA has emerged as an increasingly crucial factor in haze  
59 formation in China (Zhang et al., 2018). However, accurately modeling SOA from current chemical  
60 models is still challenging, largely attributed to our limited understanding of its formation  
61 mechanisms (Charan et al., 2019; Matsui et al., 2009; Lu et al., 2020). Thus, there is a crucial need  
62 for a comprehensive understanding of SOA formation and aging processes in the ambient  
63 environment.

64 Positive matrix factorization (PMF) has been widely used to apportion the contribution of  
65 primary and secondary sources to organic aerosol (OA) (Chen et al., 2014; Chen et al., 2021a; Ou  
66 et al., 2023; Tian et al., 2016). For the input of OA, the matrix of time serial spectral of OA measured  
67 by the Aerodyne Aerosol Mass Spectrometers (AMS) or Aerosol Chemical Speciation Monitor  
68 (ACSM) was usually applied (Uchida et al., 2019; Canonaco et al., 2013). Based on this approach,  
69 various primary OA (POA) components such as, hydrocarbon-like OA (HOA, associated with traffic  
70 emission), biomass burning OA (BBOA), cooking OA (COA), and secondary OA (SOA) with  
71 different oxidation levels are broadly identified in field measurements (Zhang et al., 2012; Jimenez  
72 et al., 2009; Huang et al., 2010; Qin et al., 2017; Guo et al., 2020; Huang et al., 2018; Al-Naiema et  
73 al., 2018). OA factors are generally distinguished according to their features on mass spectral and  
74 time series (Ulbrich et al., 2009; Lee et al., 2015). However, the electric ionization sources (70ev),  
75 together with thermal decomposition at 600C, lead to strongly fragmented ions detected in  
76 AMS/ACSM. These fragmented ions lack parent molecular information, thus hindering the ability  
77 to further attribute OA factors to more specific sources, thereby limiting our understanding of SOA  
78 formation pathways and aging mechanisms in ambient environments. To overcome this challenge,  
79 applying PMF analysis of molecular-level datasets is needed for refining SOA source apportionment.  
80 Recently, chemical ionization mass spectrometer coupled with the Filter Inlet for Gases and  
81 Aerosols (FIGAERO-CIMS) has been increasingly employed for the molecular-level  
82 characterization of oxygenated organics compounds in the gas and particle phase (Ye et al., 2021;



83 Thornton et al., 2020). Using this approach, Ye et al. (2023) employed PMF analysis to FIGAERO-  
84 CIMS data sets and found that low-NO-like pathway had a significant contribution to SOA  
85 formation in urban area.

86 Volatility, an important property of organic compounds, is frequently described as saturation  
87 mass concentration ( $C^*$ , Donahue et al., 2006). The volatility of organic compounds is closely  
88 related to its chemical characteristics, including oxidate state, number of carbons, and functional  
89 groups (Donahue et al., 2012; Donahue et al., 2011; Ren et al., 2022). The gas-particle partitioning  
90 behavior of organic compounds is largely governed by their volatility, and thus strongly influence  
91 the formation of SOA (Nie et al., 2022). Moreover, chemical processes occurring in the particle  
92 phase can alter the volatility of organic compounds. For example, high molecular weight organic  
93 compounds can form through accretion reactions, leading to a reduction in volatility (Barsanti and  
94 Pankow, 2004; Jenkin, 2004; Kroll and Seinfeld, 2008). In addition, particle phase organic  
95 compounds can be oxidized by atmospheric oxidants (e.g.,  $O_3$ , OH, and  $NO_3$ ), which can also alter  
96 the chemical characteristic and volatility (Rudich et al., 2007; Walser et al., 2007). Thus, the  
97 variation of volatility can provide valuable information about the formation and aging processes of  
98 OA. Graham et al. (2023) found that SOA from  $NO_3$  oxidation of  $\alpha$ -pinene or isoprene had a higher  
99 volatility than it from  $\beta$ -caryophyllene. Hildebrandt Ruiz et al. (2015) demonstrated that exposure  
100 to different OH levels could lead to a large variation in SOA volatility.

101 However, linking OA volatility directly to its chemical characteristics and sources remains  
102 challenging. A thermodenuder (TD) coupled with an AMS has been employed to investigate the  
103 volatility of OA from different sources (Louvaris et al., 2017). Xu et al. (2021) estimated the  
104 volatility of different PMF OA factors in the North China Plain and reported that RH level could  
105 alter both the formation pathway and volatility of more oxidized oxygenated OA. Feng et al. (2023)  
106 reported the much lower OA volatility from out plumes of North China plain than results obtained  
107 in the urban areas, signifying the aging impact on OA volatility. Nevertheless, owing to the  
108 operational principle of AMS, it is still difficult to obtain molecular information of organic  
109 compounds at different volatilities. In contrast, the FIGAERO-CIMS provides not only molecular-  
110 level measurements but also thermal desorption profiles (thermograms) for each detected compound.  
111 The temperature of the peak desorption signal ( $T_{max}$ ) of a specific compound is typically correlated  
112 with its volatility (Lopez-Hilfiker et al., 2014), enabling direct connects between the volatility and



organic molecular (Ren et al., 2022). Huang et al. (2019) analysis the ambient particles filter samples collected in different seasons with FIGAERO-CIMS and reported a lower volatility of oxygenated OA in winter, partly due to higher O:C. Buchholz et al. (2020) utilized PMF analysis of FIGAERO-CIMS thermogram data sets to investigate physicochemical property of laboratory-generated SOA particles.

To comprehensively investigate the evolution of OA and its relationship with volatility in ambient environment, we employed a FIGAERO-CIMS along with other online instruments to gain a comprehensive understanding of the variation in SOA volatility within urban plumes in the Pearl River Delta (PRD) region during the fall of 2019. PMF analysis was performed on thermograms data obtained from the FIGAERO-CIMS. By combining the source apportionment of thermogram organic aerosol (OA) with corresponding volatility information, we investigated the potential formation pathway and influencing factors of SOA in the urban downwind region.

## 2.Measurement and Method

### 2.1 Field Measurements

We conducted a field campaign at the Heshan supersite in the PRD region from September 29 to November 17, 2019. Considering the integrity of the measurements, we focus primarily on the period from October 16 to November 16, 2019 in this study. The measurement site was located in a rural area surrounded by farms and villages (at 22°42'39. 1"N, 112°55'35.9"E, with an altitude of about 40 m), situated to the southwest of the PRD region. All online instruments were placed in air-conditioned rooms on the top floor of the supersite building.

A FIGAERO-CIMS, coupled with an X-ray source, was used to measure organic compounds in both the gas- and particle-phase, utilizing I<sup>+</sup> as the chemical ionization reagent. The instrument operated on one-hour cycle by switching between two modes (sampling mode and desorption mode) for measuring gas- and particle-phase oxygenated organic molecules. In the sampling mode, ambient gas was measured in the first 21 minutes, followed by a 3-min zero air background, while the PM<sub>2.5</sub> sample was collected on a PTFE membrane filter for 24 minutes. Then, the instrument was switched to the desorption mode, in which the collected particles were desorbed using heated N<sub>2</sub>. The temperature of the N<sub>2</sub> was increased from approximately 25°C to 175°C over a 12-minute period, and then held at 175°C for an additional 24 minutes. Calibration of a few chemicals was



142 conducted in the laboratory. For the remaining organic species, a voltage scanning method was used  
143 to determine their sensitivities (referred to as semi-quantified species) (Ye et al., 2021; Iyer et al.,  
144 2016; Lopez-Hilfiker et al., 2016). The detailed operation settings, data processing, and calibration  
145 can be found in Cai et al. (2023) and Ye et al. (2021).

146 A soot particle aerosol mass spectrometer (SP-AMS, Aerodyne Research, Inc., USA) was used  
147 to measure the chemical composition of PM<sub>1</sub> particles, including nitrate, sulfate, ammonium,  
148 chloride, black carbon, and OA. More details on the quantification using ionization efficiency,  
149 composition dependent collection efficiency, data analysis, and source apportionment of OA from  
150 AMS data (defined as AMS-OA) could be found in Kuang et al. (2021) and Cai et al. (2024). In  
151 brief, AMS-OA consisted of two primary OA factors and four secondary OA factors. The primary  
152 OA factors include hydrocarbon-like OA (HOA, 11%) and biomass burning OA (BBOA, 20%),  
153 which were mainly contributed by traffic and cooking emissions and biomass burning combustion,  
154 respectively. For SOA factors, biomass burning SOA (BBSOA, 17%) was likely formed through  
155 oxidation of biomass burning emission; less oxidized oxygenated OA (LO-OOA, 24%), which  
156 results from strong daytime photochemical processes; more oxidized oxygenated OA (MO-OOA,  
157 17%), related to regional transport; and nighttime-formed OA (Night-OA, 11%) which was  
158 associated with nighttime chemistry.

159 Trace gases such as O<sub>3</sub> and NO<sub>x</sub> were measured by gas analyzers (model 49i and 42i, Thermo  
160 Scientific, US). Meteorological parameters, including wind speed and wind direction, were  
161 measured by a weather station (Vantage Pro 2, Davis Instruments Co., US).

## 162 **2.2 Methodology**

163 Positive matrix factorization (PMF) is a widely used tool for source apportionment of long  
164 timeseries data (Paatero and Tapper, 1994). In the desorption mode, the particulate organic  
165 compounds are thermo-desorbed and simultaneously measured by the FIGAERO-CIMS. Organic  
166 molecules with different volatility were characterized by thermograms (desorption signals vs  
167 temperature of N<sub>2</sub>). Here, we performed PMF analysis to the thermogram data of organic  
168 compounds measured by the FIGAERO-CIMS (FIGAERO-OA) using the Igor-based PMF  
169 Evaluation Tool (PET, v3.01, Ulbrich et al., 2009), which can be expressed as follows:

$$170 \quad \mathbf{X} = \mathbf{GF} + \mathbf{E} \quad (1)$$

171 where  $\mathbf{X}$  is the thermogram organic compound data measured by the FIGAERO-CIMS. which



172 can be decomposed into two matrices  $\mathbf{G}$  and  $\mathbf{F}$ . The matrix  $\mathbf{G}$ ,  $\mathbf{F}$ , and  $\mathbf{E}$  contain the factor time series,  
173 factor mass spectra, and the residuals between the measured data and the reconstructed data.

174 The raw normalized count per second (NCPS) thermogram data with a time resolution of 1s  
175 was averaged to a 20s-time grid, and then was background-corrected by subtracting linearly  
176 interpolated background thermogram signals. For each scan, only the data points when the  
177 desorption temperature increased were used as input data (corresponding to 25°C to 170 °C, 1-70  
178 data points in this study, Fig. S1), since the main information lies during the species desorbing from  
179 the FIGAERO filter (Fig. S1, Buchholz et al., 2020). Then, we combined data from separate  
180 thermogram scans (without background scans) to a larger input data set.

181 To perform the PMF analysis, a data uncertainty matrix ( $S_{i,j}$ ) is needed, where the  $i$  and  $j$   
182 represents the index of ions and data points, respectively. According to Buchholz et al. (2020), the  
183 uncertainty was assumed to be constant for each individual thermogram scan (constant error  
184 scheme). The  $S_{i,j}$  of a specific thermogram scan can be determined by the following equation:

$$185 \quad S_{i,j} = \sigma \quad (2)$$

186 For each thermogram scan, the last 20 data points are assumed to be in steady state. Thus, the  
187  $\sigma_{noise}$  was calculated as the median of the standard deviation of the residual ( $res_{i,j}$ ), which can be  
188 obtained from the difference between the data points ( $Data_{i,j}$ ) and the corresponding linear fitted  
189 value ( $FittedData_{i,j}$ ) for the measured data points (Fig. S2):

$$190 \quad res_{i,j} = Data_{i,j} - FittedData_{i,j} \quad (3)$$

$$191 \quad \sigma = median(stdev(res_{i,j})) \quad (4)$$

192 Due to the large volume of the data matrix (59500×1028) exceeding the processing capacity  
193 of the PET, we had to divide the data matrix into three parts and performed PMF analysis separately.  
194 The details can be found in section S1. An eight-factor solution was selected to analyze the source  
195 of FIGAERO-OA from 5 October to 16 November.

196 Since input data sets of PMF analysis were the NCPS data, the signal of each thermograms  
197 factor was a combination of NCPS values of different ions. Thus, it is necessary to convert the signal  
198 of these factors into mass concentrations, which would increase the representativeness of the  
199 thermogram PMF results. The NCPS of a specific ion was linearly correlated with the corresponding  
200 mass concentration. Thus, for a signal running cycle (a thermogram scan), the mass concentration  
201 of a specific thermograms OA factor  $k$  ( $M_k$ ) can be estimated as:



$$M_k = \sum_i \left( \frac{\sum_j \text{Signal}_{j,k} \cdot \text{Profile}_{i,k}}{\sum_j \text{NCPS}_{j,i}} \cdot m_i \right) \quad (7)$$

where  $i$  and  $j$  represent the index of species and data points; the  $\text{Signal}_{j,k}$  is the signal of a thermograms OA factor  $k$  at a data index  $j$ ; the  $\text{Profile}_{i,k}$  represents the fraction of signal of factor  $k$  and ion  $i$ ; the  $\text{NCPS}_{j,i}$  is the NCPS of species  $i$  at a data index  $j$ ; and  $m_i$  is the mass concentration of species  $i$  in the particle-phase measured by the FIGAERO-CIMS.

For a specific organic compound, the temperature of the peak desorption signal ( $T_{\max}$ ) has a nearly linear relationship with the logarithm of saturation vapor pressure ( $P_{\text{sat}}$ ) of the respective organic compound (Lopez-Hilfiker et al., 2014):

$$\ln(P_{\text{sat}}) = aT_{\max} + b \quad (8)$$

where  $a$  and  $b$  are fitting coefficients.  $P_{\text{sat}}$  can be converted to saturation vapor concentration ( $C^*$ ,  $\mu\text{g m}^{-3}$ ) by following equation:

$$C^* = \frac{P_{\text{sat}} M_w}{RT} 10^6 \quad (9)$$

where  $M_w$  is the average molecular weight of the organic compound (determined by the FIGAERO-CIMS),  $R$  is the gas constant ( $8.314 \text{ J mol}^{-1} \text{ K}^{-1}$ ), and  $T$  is the thermodynamic temperature ( $298.15 \text{ K}$ ). The fitting parameters  $a$  and  $b$  was calibrated by a series of polyethylene glycol (PEG 5-8) compounds before the campaign. The details of the calibration experiments and selection of fitting coefficients ( $a$  and  $b$ ) can be found in table S1 and Cai et al. (2024). In this study, the fitting parameters ( $a=-0.206$  and  $b=3.732$ ) was chosen, as the mass loading ( $407 \text{ ng}$ ) and diameter ( $200 \text{ nm}$ ) are closest to the ambient samples.

## 3 Results

### 3.1 Overview of FIGAERO-OA factors

In this study, the average mass concentration of FIGAERO-OA was about  $5.3 \pm 2.4 \mu\text{g m}^{-3}$ . The thermogram data sets of FIGAERO-OA were analyzed with PMF and mass concentration of each factor was estimated based on eq. (7), which provide volatility and mass concentration information of OA originating from different formation pathways. An 8-factor solution was chosen to explain the thermogram of FIGAERO-OA. These factors included six associated with daytime photochemical reactions, one related to biomass-burning, and one factor contributed by nighttime chemistry. The diurnal variation, mass spectra, and thermograms of these factors can be found in Fig. S6. The estimated volatility ( $\log_{10} C^*$ ),  $T_{\max}$ , and elemental information of all factors are





shown in table 1. Given that the thermogram data can provide volatility information of organic compounds, the identified OA factors were categorized based on their potential formation pathway, volatility, and correlation with AMS PMF factors (Table 1 and Fig. S7). For example, if the PMF factor with a  $T_{max}$  located in the ranges of low volatile organic compounds (LVOC, approximately corresponding to 78.8 °C to 112.3 °C then Fig. 1), this factor will be named after low volatility OA (LVOA). For the factors whose  $T_{max}$  is above 112.3 °C, extremely low volatility (ELVOA) will be named.

The six daytime chemistry related factors include a low volatility OA factor likely formed under high  $\text{NO}_x$  condition (Day- $\text{HNO}_x$ -LVOA, 12%), a low volatility factor contributed by gas-particle partitioning (Day-L $\text{NO}_x$ -LVOA, 11%), a low volatility and an extremely low volatility factor originating from the daytime aging process (Day-aged-LVOA and Day-aged-ELVOA, 16% and 11% respectively), and a low volatility and an extremely low volatility factors related to urban air masses (Day-urban-LVOA and Day-urban-ELVOA, 16% and 7%, respectively). These daytime factors accounted for about 76.4% of the total mass of FIGAERO-OA and demonstrated distinct daytime peak. The total mass of daytime FIGAERO-OA factors showed a strong positive correlation with LO-OOA in AMS-OA ( $R=0.86$ ), which was attributed to photochemical reactions (Fig. S7a).

Both Day- $\text{HNO}_x$ -LVOA and Day-L $\text{NO}_x$ -LVOA reached their peak values at about 14:00 LT (Fig. 1 a1 and b1), implying strong photochemical production. Day- $\text{HNO}_x$ -LVOA had the highest N:C (0.06) and the lowest oxidation state ( $\overline{OS}_c = -0.01$ ), which could be attributed to the “high  $\text{NO}_x$ ” formation pathway. It was also supported by significant positive correlation ( $R=0.93-0.94$ ) with particulate phase nitrogen-containing organic compounds (e.g.,  $\text{C}_4\text{H}_5\text{NO}_6$ ,  $\text{C}_8\text{H}_{11}\text{NO}_8$ , and  $\text{C}_8\text{H}_{11}\text{NO}_9$ ). Previous studies found that high  $\text{NO}_x$  concentration can suppress the production of molecules with a high oxidation degree (Rissanen, 2018; Praske et al., 2018), which could explain the low  $\overline{OS}_c$  value (-0.01) and relative high volatility ( $\log_{10} \overline{C}^* = -0.98$ ) found for Day- $\text{HNO}_x$ -LVOA. Day-L $\text{NO}_x$ -LVOA had a higher  $\overline{OS}_c$  (0.18) and lower  $\log_{10} \overline{C}^*$  (-2.71) than Day- $\text{HNO}_x$ -LVOA, consistent with that Day-L $\text{NO}_x$ -LVOA was composed of smaller and more oxidized non-nitrogen containing compounds (e.g.,  $\text{C}_2\text{H}_2\text{O}_3$ ,  $\text{C}_3\text{H}_4\text{O}_3$ ,  $\text{C}_4\text{H}_6\text{O}_4$ , and  $\text{C}_6\text{H}_8\text{O}_4$ ). Noting that C2-C3 group could originate from the decomposition of larger molecules during thermal desorption, since the thermogram demonstrated a bimodal distribution (Fig. 1 b3) and  $\text{C}_2\text{H}_2\text{O}_3$  and  $\text{C}_3\text{H}_4\text{O}_3$  had a relatively high  $T_{max}$  (Fig. S9a).



261 Additionally, we identified two aged OA factors (Day-aged-LVOA and Day-aged-ELVOA)  
262 with an afternoon peak at about 18:00 LT (Fig. 1 c1 and d1), which may be derived from the aging  
263 transformation of preexisting organic aerosols via daytime photochemical reactions. These aged  
264 factors exhibited the highest  $\overline{OS_c}$  (0.35 and 0.40) and relatively low volatility with a  $\log_{10} C^*$  of -  
265 2.02 and -4.80, respectively. Day-aged-LVOA was featured with a series of C<sub>4</sub>-C<sub>8</sub> oxygenated  
266 compounds (e.g., C<sub>4</sub>H<sub>6</sub>O<sub>5</sub>, C<sub>5</sub>H<sub>8</sub>O<sub>5</sub>, C<sub>6</sub>H<sub>10</sub>O<sub>5</sub>, C<sub>7</sub>H<sub>10</sub>O<sub>5</sub>, and C<sub>8</sub>H<sub>12</sub>O<sub>5</sub>). In contrast, Day-aged-  
267 ELVOA had a higher fraction of smaller molecules (e.g., C<sub>2</sub>H<sub>4</sub>O<sub>3</sub> and C<sub>3</sub>H<sub>6</sub>O<sub>3</sub>, Fig. 1d2). Chen et  
268 al. (2021b) found that low molecular weight carboxylic acids (LMWCA) could form through SOA  
269 aging processes and report a strong correlation ( $R^2=0.90$ ) between LMWCA and highly oxygenated  
270 OA. However, C<sub>2</sub>H<sub>4</sub>O<sub>3</sub> had a weak correlation ( $R=0.49$ ) with MO-OOA resolved from AMS. In  
271 addition, the  $T_{max}$  of C<sub>2</sub>H<sub>4</sub>O<sub>3</sub> located in the ELVOC range and C<sub>2</sub>H<sub>4</sub>O<sub>3</sub> has a similar thermogram  
272 with Day-aged-ELVOA (Fig. S9), supporting C<sub>2</sub>H<sub>4</sub>O<sub>3</sub> was more likely decomposition product of  
273 low-volatile organic compounds rather than directly formed through aging process.

274 Two urban air masses-related OA factors (Day-urban-LVOA and Day-urban-ELVOA) were  
275 identified, which would be discussed in the following section. Day-urban-LVOA demonstrated  
276 comparable  $\overline{OS_c}$  (0.08), O:C (0.80) and volatility (-0.90) to Day-HNO<sub>x</sub>-LVOA (-0.01, 0.75, and -  
277 0.98, respectively), but show a higher fraction of non-N-containing molecules (e.g., C<sub>4</sub>H<sub>6</sub>O<sub>4</sub>,  
278 C<sub>5</sub>H<sub>6</sub>O<sub>4</sub>, C<sub>5</sub>H<sub>8</sub>O<sub>5</sub>, and C<sub>7</sub>H<sub>10</sub>O<sub>5</sub>) and a reduced N:C ratio (Table 1). Day-urban-ELVOA had the  
279 lowest volatility ( $\log_{10} C^* = -7.18$ ) but an  $\overline{OS_c}$  (0.27) lower than Day-aged-ELVOA (0.34) and  
280 composed of oxygenated compounds (e.g., C<sub>8</sub>H<sub>10</sub>O<sub>5</sub>, C<sub>7</sub>H<sub>8</sub>O<sub>5</sub>, C<sub>6</sub>H<sub>8</sub>O<sub>4</sub>, and C<sub>5</sub>H<sub>6</sub>O<sub>4</sub>). The  
281 thermogram of Day-aged-ELVOA demonstrates bimodal distribution (peaked at LVOC and  
282 ELVOC range) and had a highest  $T_{max}$  (153.2 °C) among thermograms OA factors (Fig. 1f3).  
283 However, the majority of organic molecules in Day-urban-ELVOA did not show a similar  
284 thermogram to Day-urban-ELVOA (Fig. S10), which had a minor contribution to the thermogram  
285 peak located at ELVOC range. It indicates that this peak might be mainly contributed by  
286 decomposition products.

287 The biomass-burning related factor, biomass-burning less volatile organic aerosol (BB-LVOA,  
288 10% of FIGAERO-OA), had a low  $\overline{OS_c}$  (-0.07), the lowest O:C (0.74), and positive correlation with  
289 BBOA resolved from AMS ( $R=0.64$ , Fig. S7b). It presented a prominent peak at 19:00 LT and was  
290 identified by the distinctive tracer levoglucosan (C<sub>6</sub>H<sub>10</sub>O<sub>5</sub>), nitrocatechol (C<sub>6</sub>H<sub>5</sub>NO<sub>4</sub>), and



nitrophenol ( $C_6H_5NO_3$ , Fig. 1) in the spectrum, which was frequently detected in biomass burning plumes (Gaston et al., 2016; Ye et al., 2021). In the upwind urban region of Heshan site, Ye et al. (2023) identified a biomass burning related factor in Guangzhou city using the FIGAERO-CIMS, with a distinct evening peak at 21:00 LT and more abundance oxygenated compounds (e.g.,  $C_7H_{10}O_5$  and  $C_8H_{12}O_6$ ). The different oxidation level of BBOA between Guangzhou and Heshan, suggest the BB-LVOA in this study is more related to the direct BB emission, but the BB factor in Guangzhou is more resembled BB related SOA factor. This statement was supported by the fact that biomass burning activities were frequently observed near the measurement site during this study, while the biomass burning activities in urban areas was prohibited and can be transported from nearby suburban agricultural areas (Cai et al. 2023).

The nighttime chemistry related less volatile OA (Night-OA, 15% of FIGAERO-OA) has the highest N:C (0.07) and exhibited an enhanced at nighttime (22:00-24:00 LT, Fig. 1). Notably, this nighttime factor was composed of a series of organic nitrates (e.g.,  $C_8H_{11}NO_7$ , and  $C_{10}H_{15}NO_7$ ), which was related to the products from monoterpenes oxidized by the  $NO_3$  radical or oxidation of biomass burning products during nighttime (Faxon et al., 2018; Decker et al., 2019). Noting that the levoglucosan ( $C_6H_{10}O_5$ ) was also abundant in the Night-LVOA, suggesting that part of this factor could be attributed to the nighttime aging process of biomass burning products (Jorga et al., 2021). The detailed discussion about the potential formation pathway of these six daytime FIGAERO-OA factors will be discussed in section 3.2.

The volatility of organic compounds was closely related to their chemical characteristics (Donahue et al., 2012). Figure 2 demonstrates the relationship between  $\log_{10} \overline{C^*}$  of thermogram factors and  $\overline{OS_c}$ , O:C, and number of carbons ( $nC$ ). In general, these factors exhibited a negative correlation ( $R=-0.60$  and  $-0.73$ ) with both the  $\overline{OS_c}$  and the O:C but showed a positive correlation ( $R=0.73$ ) with  $nC$  (Fig. 2), except for Day-urban-ELVOA. As aforementioned, the major component of Day-urban-ELVOA could be decomposition products of larger oxygenated molecules. Thus, the chemical characteristic of Day-urban-ELVOA did not demonstrate a similar relationship of volatility versus molecule indicators (e.g., oxidation state, O:C and  $nC$ ) as other factors. The increase of carbon number usually lead to a decrease in volatility (Donahue et al., 2011), while this trend overturned in this campaign (Fig. 2c). Fig. 2d shows that  $\overline{OS_c}$  had a negative relationship ( $R=-0.84$ ) with carbon number, suggesting that organic factors with a higher oxidation degree had a shorted



carbon backbone. It could be partly owing to fragmentation of organic molecules during aging processes (Chacon-Madrid and Donahue, 2011; Jimenez et al., 2009). Consistently, two aged factors (Day-aged-LVOA and Day-aged-ELVOA) had a higher  $\overline{OS_c}$  and a lower carbon number than other factors. Additionally, it indicates that the increase in oxidation degree outweighed the effect of decreasing  $nC$ , leading to a reduction in the volatility of OA during this campaign.

The temporal variation of volatility distribution and mean  $C^*$  of FIGAERO-OA, the sum of six daytime factors in FIGAERO-OA and LOOA in AMS OA, mass fraction of eight FIGAERO-OA factors, and wind direction and speed are demonstrated in Fig. 3. As shown in Fig. 3, the increase of mean  $C^*$  during the daytime (6:00 LT to 18:00 LT, Fig. S11 a) is usually accompanied by the enhancement of daytime factors in FIGAERO-OA and LO-OOA from AMS (Fig. S11 b and c), indicating that the formation of these factors could notably increase OA volatility. Notably, FIGAERO-OA with a  $\log_{10} C^*$  of  $-1 \mu\text{g m}^{-3}$  showed pronounced enhancements during the increasing of mean  $C^*$ , implying that the volatility of six daytime factors might cluster around  $10^{-1} \mu\text{g m}^{-3}$  (Fig. S11d). In Fig. 3b, distinct diurnal variation of  $O_x$  ( $O_x=O_3+NO_2$ ) was observed during the campaign. The maximum of  $O_x$  can be as high as  $230 \mu\text{g m}^{-3}$ , highlighting strong photochemical reaction. The daytime factors, especially Day- $HNO_x$ -LVOA (Fig. 3c), exhibited markable enhancements under weak northwesterly to northeasterly wind (Fig. 3d and Fig. S12). A backward trajectory analysis revealed that the measurement site was mainly affected by the urban pollutants from the city cluster around Guangzhou (Fig. S13). Two periods, which were long-range transport and urban air mass periods, respectively, were selected to further analyze the impact of urban pollutants on the formation and aging process of OA. The variation of OA volatility based on wind direction and speed, together with backward trajectory analysis, were also explored (Fig. S13 and Table S2). In general, during the urban air masses period, the site was influenced by regional urban plumes from the northeast city cluster, while the long-range transport period was primarily associated with air masses advected from the northeast inland regions. More detailed discussion will be shown in the following section.

### 3.2 Potential formation pathway of FIGAERO-OA

Figure 4 demonstrates distinct differences in the diurnal variation of thermograms factors (including Day- $HNO_x$ -LVOA, Day-aged-LVOA, Day-urban-LVOA, and Day-urban-ELVOA) during long-range transport period and urban air masses period. During the urban air masses period,



Day- $\text{HNO}_x$ -LVOA significantly increased from  $\sim 0.4 \mu\text{g m}^{-3}$  to  $\sim 4.8 \mu\text{g m}^{-3}$  in the daytime. The mass concentration of Day-urban-LVOA and Day-urban-ELVOA demonstrated daytime enhancements only during urban period, suggesting that the formation of these factors was closely related to the pollutants in the urban plumes. Consistently, During the urban air masses period, the maximum ozone concentration in the afternoon (12:00-18:00 LT,  $208.3 \mu\text{g m}^{-3}$ ) was higher than that ( $185.5 \mu\text{g m}^{-3}$ ) during long-range transport period, indicating a stronger photochemical reaction in the urban plumes (Fig. 4). Thus, the daytime thermogram factors accounted for a higher fraction (79% vs 75%) of FIGAERO-OA (Fig. S14). Additionally, the average mass concentration of all thermogram factors ( $8.9 \pm 5.1 \mu\text{g m}^{-3}$ ) was noticeably increased compared to the long-range period ( $5.3 \pm 2.4 \mu\text{g m}^{-3}$ ). Elevated  $\text{NO}_x$  concentration was observed in the urban plumes in the afternoon (12:00 LT-18:00 LT, 17.4 ppbv vs 11.7 ppbv), which might also affect the formation pathway of SOA. Both NO and NO/ $\text{NO}_2$  remained at a relative low level (0.6-0.8 ppbv and  $<0.5$ ) in the afternoon during these two periods (Fig. S15), suggesting an important role of low-NO-like pathway (Ye et al., 2023). Nihill et al. (2021) found that the production of OH and oxidized organic molecules would be suppressed under high NO/ $\text{NO}_2$  ( $>1$ ) condition. Notably, Day- $\text{HNO}_x$ -LVOA accounted for the largest portion (29%) of FIGAERO-OA in the afternoon (12:00-18:00 LT, Fig. S16), followed by Day-aged-LVOA (21%), while Day-L $\text{NO}_x$ -LVOA contributed only 6%. In contrast, during the long-range transport period, the mass fraction of Day-L $\text{NO}_x$ -LVOA significantly increased (from 6% to 15%) along with a decrease in Day- $\text{HNO}_x$ -LVOA (from 29% to 21%). These results indicate that elevated  $\text{NO}_x$  concentration in urban plumes might alter the formation pathway of SOA (Cai et al., 2024).

To explore the potential formation pathway of daytime factors, figure 5 demonstrates the variation of mass concentrations of six daytime factors as a function of  $\text{O}_x$ , total gas-phase organic molecules measured by the FIGAERO-CIMS (referred as organic vapors), and  $\text{NO}_3^-/\text{SIA}$ . Five factors, excluding Day-urban-LVOA, exhibited positive correlations with  $\text{O}_x$ , highlighting the critical role of photochemical reactions in their formation. Previous studies have demonstrated that gas-particle partitioning plays a key role in SOA formation (Nie et al., 2022; Wang et al., 2022). In this study, organic vapors had strong positive correlations with Day- $\text{HNO}_x$ -LVOA ( $R=0.73$ ) and Day-L $\text{NO}_x$ -LVOA ( $R=0.74$ ), suggesting that these factors were mainly formed via gas-particle partitioning. The median concentration of Day- $\text{HNO}_x$ -LVOA dramatically increased (from  $\sim 0$  to



381  $\sim 5.6 \mu\text{g m}^{-3}$ ) with rising organic vapors, whereas a comparable enhancement was not observed for  
382 Day-LNO<sub>x</sub>-LVOA (Fig. 5 b1 and b2).

383 Furthermore, NO<sub>x</sub> impact on Day-HNO<sub>x</sub>-LVOA and Day-LNO<sub>x</sub>-LVOA was investigated here.  
384 Fig. S17 show Day-HNO<sub>x</sub>-LVOA concentrations were consistently higher under elevated NO<sub>x</sub>  
385 conditions, while Day-HNO<sub>x</sub>-LVOA decreased with increasing NO<sub>x</sub> level. Figure 6a displays the  
386 mass ratio of Day-HNO<sub>x</sub>-LVOA to Day-LNO<sub>x</sub>-LVOA obviously increased with organic vapors (up  
387 to 12~26) under high NO<sub>x</sub> condition ( $>20$  ppbv), while the ratio remained at approximately 2 at  
388 low NO<sub>x</sub> level ( $<10$  ppbv). These overall results suggest that Day-HNO<sub>x</sub>-LVOA formation was  
389 predominantly governed by gas-particle partitioning under high NO<sub>x</sub> condition, which were  
390 typically sustained during urban air masses period (Fig. 2d). Figure 6b compares the relative mass  
391 fraction of molecular composition in two gas-particle partitioning related factors, Day-HNO<sub>x</sub>-  
392 LVOA and Day-LNO<sub>x</sub>-LVOA. The mass fraction of species was derived from the signal profile of  
393 corresponding factors based on their sensitivity (Ye et al., 2021). Day-HNO<sub>x</sub>-LVOA presented  
394 greater proportions ( $10^{-5}\sim 10^{-3}$ ) of organic nitrates (ONs) than Day-LNO<sub>x</sub>-LVOA ( $10^{-11}\sim 10^{-9}$ ),  
395 including C<sub>4</sub>H<sub>7</sub>NO<sub>6</sub>, C<sub>8</sub>H<sub>9</sub>NO<sub>4</sub>, C<sub>8</sub>H<sub>11</sub>NO<sub>7</sub>, as well as nitrophenols (e.g., C<sub>7</sub>H<sub>7</sub>NO<sub>3</sub>), which are  
396 characterized by relatively low  $\overline{OS}_C$ . These compounds were probably attributed to the SOA  
397 formation under elevated NO<sub>x</sub> concentration (Fig. 2d). In contrast, Day-LNO<sub>x</sub>-LVOA was enriched  
398 in non-nitrogen-containing species (e.g., C<sub>4</sub>H<sub>6</sub>O<sub>3</sub>, C<sub>5</sub>H<sub>10</sub>O<sub>3</sub>, C<sub>11</sub>H<sub>17</sub>O<sub>6</sub>), which exhibited a higher  
399  $\overline{OS}_C$ . These results indicate that NO<sub>x</sub> exerts contrasting effects on the formation of these two gas-  
400 particle partitioning-related factors.

401 Previous studies show that NO<sub>x</sub> has a nonlinear effect on the formation of highly oxygenated  
402 organic (HOM) compounds by influencing the atmospheric oxidation capacity and RO<sub>2</sub>  
403 autoxidation (Xu et al., 2025; Pye et al., 2019; Shrivastava et al., 2019). NO<sub>x</sub> could suppress the  
404 production of low-volatility molecules by inhibiting autoxidation (Rissanen, 2018; Praske et al.,  
405 2018), while Nie et al. (2023) found that NO could enhance the formation of HOM at low NO  
406 condition ( $<82$  pptv). During this campaign, the average NO<sub>x</sub> and NO was about 24.0 ppbv and 2.3  
407 ppbv, respectively, substantially higher than the “low-NO-regime” described by Nie et al. (2023).  
408 Our previous study reported a lower concentration of organic vapors with a high  $\overline{OS}_C$  within urban  
409 plumes during the same campaign (Cai et al., 2024). Furthermore, as illustrated in Fig. S18, the  
410 mass concentration of SVOC ( $-0.5 < \log_{10} C^* < 2.5 \mu\text{g m}^{-3}$ ) and LVOC ( $-3.5 < \log_{10} C^* < -0.5 \mu\text{g m}^{-3}$ )



<sup>3</sup>, Donahue et al., 2012) in the gas phase exhibited an increase ( $2.5 \mu\text{g m}^{-3}$  at  $\text{NO}_x < 10$  ppbv vs  $3.3 \mu\text{g m}^{-3}$  at  $\text{NO}_x \geq 30$  ppbv) with the increase in  $\text{NO}_x$ , suggesting that these species likely contributed to the formation of Day- $\text{HNO}_x$ -LVOA. Figure 5 c1 and c2 investigate the relationship between these two factors and  $\text{NO}_3^-/\text{SIA}$ . Day- $\text{HNO}_x$ -LVOA had a weak correlation ( $R=0.30$ ) with  $\text{NO}_3^-/\text{SIA}$ , while this trend overturned ( $R=-0.35$ ) for Day-L $\text{NO}_x$ -LVOA. Yang et al. (2022) showed that  $\text{OH}+\text{NO}_2$  pathway mainly contribute to the formation of nitrate in this campaign. Together, these results indicate that elevated  $\text{NO}_x$  suppressed the formation of highly oxygenated organic compounds, thereby limiting the contribution to Day-L $\text{NO}_x$ -LVOA. Thus, the Day-L $\text{NO}_x$ -LVOA was more likely formed via gas-particle partitioning under relatively low  $\text{NO}_x$  condition.

It is worth noting that  $\text{C}_4\text{H}_7\text{NO}_5$ , likely originating from isoprene photooxidation in the presence of  $\text{NO}_x$  (Fisher et al., 2016; Paulot et al., 2009), also show a higher fraction in Day-L $\text{NO}_x$ -LVOA ( $9.36 \times 10^{-5}$  vs  $4.93 \times 10^{-11}$  in Day- $\text{HNO}_x$ -LVOA). A plausible explanation is that Heshan site, located at a suburban region, experienced ambient  $\text{NO}_x$  levels ( $\sim 13$  ppb in the afternoon) sufficient to facilitate the formation of  $\text{C}_4\text{H}_7\text{NO}_5$ . It is further supported by the observation that both particle- and gas-phase  $\text{C}_4\text{H}_7\text{NO}_5$  showed no significant variation with increasing  $\text{NO}_x$  (Fig. S19).

For the two urban-related factors, a positive correlation with  $\text{O}_x$  was observed only during the urban air masses period ( $R=0.46$  and  $0.64$  vs  $-0.05$  and  $0.28$  in the long-range transport period, Fig. S19 a and c). Notably, Day-urban-LVOA increased from  $\sim 1.0$  to  $\sim 2.6 \mu\text{g m}^{-3}$  as  $\text{O}_x$  rose from  $75$  to  $275 \mu\text{g m}^{-3}$  during this period, while it remained relatively stable ( $\sim 0.4 \mu\text{g m}^{-3}$ ) during the long-range transport period (Fig. S20). This finding supports the hypothesis that the daytime formation of urban-related OA factors was closely related to the urban pollutants. Additionally, Day-urban-ELVOA exhibited a positive correlation with organic vapors ( $R = 0.65$ , Fig. S20b), while such a correlation was not observed for Day-urban-LVOA. It implies that Day-urban-ELVOA may primarily form through gas-particle partitioning during the urban air mass period.

Day-urban-LVOA was also positively correlated with  $\text{NO}_3^-/\text{SIA}$  (Fig. 5c), consistent with the concurrent enhancement of nitrate and SOA during haze episodes (Ye et al., 2023; Zheng et al., 2021). During the urban air masses period, nitrate demonstrates a bimodal diurnal variation with peaks in both the morning and afternoon (Fig. S21), the latter peak likely attributed to  $\text{OH}+\text{NO}_2$  pathway (Yang et al., 2022). Day-urban-LVOA had a significant correlation ( $R=0.97$ ) with succinic acid ( $\text{C}_4\text{H}_6\text{O}_4$ ) in the particle phase (Fig. S22), which was previously reported to form via



441 multiphase reaction during haze episode in megacity (Zhao et al., 2018; Zheng et al., 2021). As  
442 shown in Fig. S23, Day-urban-LVOA also increased with the ratio of the aerosol liquid water  
443 content (ALWC) to  $PM_{10}$ , further indicating that aqueous processes in urban plumes played an  
444 important role in its enhancement.

445 For the aging factors, Day-aged-LVOA and Day-aged-ELVOA exhibited peak concentrations  
446 about 3 hours later (at about 18:00 LT, Fig. 4) than other day factors (15:00 LT). It suggests that the  
447 two aged factors might originate from the photochemical aging processes of preexisting organic  
448 aerosols. To further explore the formation and aging process of these daytime factors, we estimated  
449 their daytime enhancement ( $\Delta$ ). For factors peaked at 15:00 LT, the  $\Delta$  was estimated as the difference  
450 between the average mass concentration during 00:00-6:00 LT and 12:00-18:00 LT. For factors  
451 peaking at about 18:00 LT,  $\Delta$  was regarded as the difference between the average mass  
452 concentration during 6:00-12:00 LT and 15:00-21:00 LT, since these factors remained at a relatively  
453 high-level during nighttime probably owing to lower boundary layer height. The  $\Delta$  Day-aged-  
454 LVOA showed strong positive correlations with  $\Delta$  Day- $HNO_x$ -LVOA ( $R=0.73$ ),  $\Delta$  Day-urban-  
455 LVOA ( $R=0.77$ ), and  $\Delta$  Day- $LNO_x$ -LVOA ( $R=0.64$ , Fig. 7a), suggesting that its formation might  
456 be closely associated with the aging processes of these three factors. Similarly,  $\Delta$  Day-aged-ELVOA  
457 was positively correlated with both  $\Delta$  Day- $LNO_x$ -LVOA ( $R=0.61$ ),  $\Delta$  Day-urban-LVOA ( $R=0.67$ ),  
458 and  $\Delta$  Day-urban-ELVOA ( $R=0.73$ , Fig. 7c). In contrast, we did not observe such correlations  
459 between  $\Delta$  Day-aged-ELVOA and  $\Delta$  Day- $HNO_x$ -LVOA ( $R=0.49$ , Fig. 7c). It implies that the  
460 formation of Day-aged-ELVOA was likely more influenced by the aging of urban-related factors  
461 and Day- $LNO_x$ -LVOA.

### 462 3.3 Comparison with AMS OA

463 Adopting PMF analysis to thermogram datasets provides valuable insights into the formation  
464 and aging processes of SOA. However, the representativeness of FIGAERO-OA still requires  
465 evaluation. Figure 8 compares FIGAERO-OA with AMS-OA during two different periods. In  
466 general, FIGAERO-OA could not explain MO-OOA and HOA identified in AMS OA, given that  
467 all thermogram factors had a weak correlation ( $R=-0.18-0.36$ ) between these two factors (Table S2).  
468 MO-OOA, which had the highest O:C (1.0) among all AMS factors (0.32-1.0) (Cai et al., 2024),  
469 was likely low volatile, meaning that much of this fraction might not have been vaporized during  
470 the heating process. HOA mainly consists of hydrocarbon-like organic compounds, which could not





471 be detected by the FIGAERO-CIMS.

472 BBSOA in AMS-OA had a bimodal diurnal distribution with an afternoon peak (~ 14:00 LT)  
473 and an evening peak (~ 17:00 LT, Fig. S24). The enhancement was more pronounced in the  
474 afternoon (~1.6 to ~ 3.6  $\mu\text{g m}^{-3}$ ) compared to the evening (~2.9 to ~4.0  $\mu\text{g m}^{-3}$ ). Thus, we classify  
475 both BBSOA and LOOA as daytime SOA. Six thermogram daytime factors could explain the  
476 majority (82% on average) of daytime SOA with the explained fraction increasing from 78% during  
477 the long-range transport period to 85% during the urban air masses period (Fig. 8 a and b). In both  
478 periods, the summed thermogram daytime factors exhibited a diurnal variation like that of  
479 LOOA+BBSOA (Fig. 8 c and d). Thermogram daytime OA was close to AMS daytime OA in the  
480 morning but fell below AMS OA afternoon. The discrepancy in the afternoon could be related to  
481 the decrease in OA volatility through strong photochemical reactions. Since the heating temperature  
482 of the FIGAERO-CIMS was set at 175°C, compounds of very low volatility might not have been  
483 fully detected. This discrepancy narrowed during the urban air masses, likely owing to the strong  
484 SOA formation through gas-particle partitioning, which increased OA volatility (Cai et al., 2024).  
485 The gap persisted overnight, owing to suppressed vertical mixing under lower boundary layer  
486 conditions.

487 FIGAERO-OA explained about 13% of BBOA in AMS OA during the campaign and this ratio  
488 remained relatively stable across different periods compared with daytime SOA (Fig. 8 a and b).  
489 Because BBOA is closely tied to local biomass burning activities, air mass variations likely had  
490 only a minor influence on its chemical characteristics. BB-LVOA showed a diurnal pattern similar  
491 to both BBOA in AMS-OA and levoglucosan (Fig. 9a), with an evening peak around 18:30 LT,  
492 confirming their close association with biomass burning emissions. For nighttime chemistry related  
493 factor, both Night-OA (from AMS) and Night-LVOA (from thermograms) increase during the  
494 nighttime, while they did not share a similar diurnal pattern (Fig. 9b). Night-LVOA peaked at about  
495 20:00 LT and decreased after 4:00 LT, while Night-OA peaked later, at about 06:00 LT, and declined  
496 in the morning. It suggested that Night-LVOA identified by FIGAERO-CIMS might not be able to  
497 fully capture the evolution of organic compounds involved in nighttime chemistry, which can  
498 explain 48% of Night-OA in AMS-OA. Given that the majority of organic compounds formed  
499 through the nighttime chemistry were oxygenated and could be detected by FIGAERO CIMS (Wu  
500 et al., 2021), we speculated that the volatility of organic compounds decreased overnight, resulting



501 that some low volatility organic aerosols would not be fully vaporized during the heating process.

## 502 **4. Conclusion**

503 In this study, we applied a PMF analysis to field thermogram data set measured by the  
504 FIGAERO-CIMS and classified the factors based on their potential formation pathways and  
505 volatility. Based on the PMF analysis to thermograms data sets, six daytime OA factors, a biomass  
506 burning related factor, and nighttime chemistry related factor were identified. The formation of Day-  
507  $\text{HNO}_x$ -LVOA and Day-L $\text{NO}_x$ -LVOA was closely related to gas-particle partitioning, while Day-  
508  $\text{HNO}_x$ -LVOA was observed to be formed with organic vapors under high  $\text{NO}_x$  condition. The  
509 increase in  $\text{NO}_x$  concentration might inhibit the production of highly oxygenated compounds (Cai  
510 et al., 2024), which could explain the relatively high volatility of Day- $\text{HNO}_x$ -LVOA. Two urban  
511 related factors, Day-urban-LVOA and Day-urban-ELVOA, were identified, which only showed a  
512 daytime enhancement in urban plumes. The former might originate from aqueous processes, while  
513 the latter was likely formed through gas-particle partitioning. Our results demonstrated that  
514 photochemical-derived gas-particle partitioning mainly contributed to OA formation in downwind  
515 urban plumes.

516 Daytime aging processes of organic aerosol were observed and leading to the decrease in  
517 volatility with two aged factors (Day-aged-LVOA and Day-aged-ELVOA) identified. The formation  
518 of Day-aged-LVOA was related to the photochemical aging processes of Day- $\text{HNO}_x$ -LVOA, Day-  
519 L $\text{NO}_x$ -LVOA, Day-urban-LVOA, and Day-urban-ELVOA, while Day-aged-ELVOA originates  
520 from the aging processes of Day-L $\text{NO}_x$ -LVOA, Day-urban-LVOA, and Day-urban-ELVOA. In  
521 general, these six thermogram daytime factors could explain the majority of daytime SOA in AMS  
522 OA, and this ratio increase from 79% during the long-range transport period to 85% during the  
523 urban air masses period, probably owing to a higher OA volatility (Cai et al., 2024). While  
524 FIGAERO-OA is unable to explain hydrocarbon like OA (HOA) and more oxygenated OA (MOOA),  
525 since the FIGAERO-CIMS could not detect hydrocarbon molecules and low volatility organic  
526 compounds with a volatilization temperature higher than 170 °C. For biomass-related OA, BB-  
527 LVOA could explain about 11%-13% of the BBOA in AMS OA, sharing a similar diurnal pattern,  
528 indicating that adopting a PMF analysis to thermogram profile could capture biomass burning events.



529 While Night-LVOA had a different diurnal pattern with Night-OA in AMS OA, implying that this  
530 thermogram factor was not unable to represent the evolution of OA during the nighttime.

531 Our results reveal that applying a PMF analysis to thermogram profiles in field campaign could  
532 provide additional volatility information, which will benefit in OA source apportionment. Along  
533 with PMF analysis of AMS or ACSM data, it can provide crucial information in understanding the  
534 formation and aging processes of OA. Using this method, we found that the daytime atmospheric  
535 evolution of SOA involved gas–particle partitioning, aqueous-phase reactions, and photochemical  
536 aging, highlighting the complexity of daytime SOA formation. Moreover, SOA volatility was  
537 strongly dependent on its formation pathways. variations in NO<sub>x</sub> not only influenced atmospheric  
538 oxidation but also modified SOA volatility by altering formation mechanisms. Nevertheless, further  
539 investigations are required to clarify the role of urban plumes in shaping SOA formation and its  
540 physicochemical properties.

541

542

543 *Data availability.* Data from the measurements are available at [10.6084/m9.figshare.30155584](https://doi.org/10.6084/m9.figshare.30155584)

544

545 *Supplement.* The supplement related to this article is available online at xxx.

546

547 *Author contributions.* M.C., W. H., and B.Y. designed the research. M.C., B.Y., W.H., Y.C., S. H.,  
548 S.Y., W.C., Y. P., and J.Z. performed the measurements. M. C., B.Y., W.H., Y.C., S. H., Z. D., and  
549 D. C. analyzed the data. M. C., W.H. and B.Y. wrote the paper with contributions from all co-authors.

550

551 *Competing interests.* The authors declare that they have no conflict of interest.

552

553 *Financial support.* This work was supported by Guangdong Basic and Applied Basic Research  
554 Foundation (grant nos. 2024A1515030221, 2023A1515012240), National Natural Science  
555 Foundation of China (grant no. 42305123, 42375105), Science and Technology Projects in  
556 Guangzhou (grant no. 2025A04J4493), the Key Innovation Team of Guangdong Meteorological  
557 Bureau (No. GRMCTD202506-ZD06) , and Central Public interest Scientific Institution Basal



558 Research Fund of South China Institute of Environmental Sciences, MEE (grant no. PM-zx097-

559 202506-214).

560



## 561 Reference

- 562 Al-Naiema, I. M., Hettiyadura, A. P. S., Wallace, H. W., Sanchez, N. P., Madler, C. J., Cevik, B. K.,  
563 Bui, A. A. T., Kettler, J., Griffin, R. J., and Stone, E. A.: Source apportionment of fine particulate matter  
564 in Houston, Texas: insights to secondary organic aerosols, *Atmos. Chem. Phys.*, 18, 15601-15622,  
565 10.5194/acp-18-15601-2018, 2018.
- 566 Apte, J. S., Brauer, M., Cohen, A. J., Ezzati, M., and Pope, C. A., III: Ambient PM<sub>2.5</sub> Reduces  
567 Global and Regional Life Expectancy, *Environmental Science & Technology Letters*, 5, 546-551,  
568 10.1021/acs.estlett.8b00360, 2018.
- 569 Arias, P. A., Bellouin, N., Coppola, E., Jones, R. G., Krinner, G., Marotzke, J., Naik, V., Palmer, M.  
570 D., Plattner, G. K., Rogelj, J., Rojas, M., Sillmann, J., Storelvmo, T., Thome, P. W., Trewin, B., Achuta  
571 Rao, K., Adhikary, B., Allan, R. P., Armour, K., Bala, G., Barimalala, R., Berger, S., Canadell, J. G.,  
572 Cassou, C., Cherchi, A., Collins, W., Collins, W. D., Connors, S. L., Corti, S., Cruz, F., Dentener, F. J.,  
573 Dereczynski, C., Di Luca, A., Diongue Niang, A., Doblas-Reyes, F. J., Dosio, A., Douville, H.,  
574 Engelbrecht, F., Eyring, V., Fischer, E., Forster, P., Fox-Kemper, B., Fuglestad, J. S., Fyfe, J. C., Gillett,  
575 N. P., Goldfarb, L., Gorodetskaya, I., Gutierrez, J. M., Hamdi, R., Hawkins, E., Hewitt, H. T., Hope, P.,  
576 Islam, A. S., Jones, C., Kaufman, D. S., Kopp, R. E., Kosaka, Y., Kossin, J., Krakovska, S., Lee, J. Y., Li,  
577 J., Mauritsen, T., Maycock, T. K., Meinshausen, M., Min, S. K., Monteiro, P. M. S., Ngo-Duc, T., Otto,  
578 F., Pinto, I., Pirani, A., Raghavan, K., Ranasinghe, R., Ruane, A. C., Ruiz, L., Sallée, J. B., Samset, B.  
579 H., Sathyendranath, S., Seneviratne, S. I., Sörensson, A. A., Szopa, S., Takayabu, I., Tréguier, A. M., van  
580 den Hurk, B., Vautard, R., von Schuckmann, K., Zaehle, S., Zhang, X., and Zickfeld, K.: Technical  
581 Summary, in: *Climate Change 2021: The Physical Science Basis. Contribution of Working Group I to*  
582 *the Sixth Assessment Report of the Intergovernmental Panel on Climate Change*, edited by: Masson-  
583 Delmotte, V., Zhai, P., Pirani, A., Connors, S. L., Péan, C., Berger, S., Caud, N., Chen, Y., Goldfarb, L.,  
584 Gomis, M. I., Huang, M., Leitzell, K., Lonnoy, E., Matthews, J. B. R., Maycock, T. K., Waterfield, T.,  
585 Yelekçi, O., Yu, R., and Zhou, B., Cambridge University Press, Cambridge, United Kingdom and New  
586 York, NY, USA, 33–144, 10.1017/9781009157896.002, 2021.
- 587 Barsanti, K. C. and Pankow, J. F.: Thermodynamics of the formation of atmospheric organic  
588 particulate matter by accretion reactions—Part 1: aldehydes and ketones, *Atmospheric Environment*, 38,  
589 4371-4382, <https://doi.org/10.1016/j.atmosenv.2004.03.035>, 2004.
- 590 Buchholz, A., Ylisirniö, A., Huang, W., Mohr, C., Canagaratna, M., Worsnop, D. R., Schobesberger,  
591 S., and Virtanen, A.: Deconvolution of FIGAERO-CIMS thermal desorption profiles using positive  
592 matrix factorisation to identify chemical and physical processes during particle evaporation, *Atmos.*  
593 *Chem. Phys.*, 20, 7693-7716, 10.5194/acp-20-7693-2020, 2020.
- 594 Cai, M., Ye, C., Yuan, B., Huang, S., Zheng, E., Yang, S., Wang, Z., Lin, Y., Li, T., Hu, W., Chen,  
595 W., Song, Q., Li, W., Peng, Y., Liang, B., Sun, Q., Zhao, J., Chen, D., Sun, J., Yang, Z., and Shao, M.:  
596 Enhanced daytime secondary aerosol formation driven by gas–particle partitioning in downwind urban  
597 plumes, *Atmos. Chem. Phys.*, 24, 13065-13079, 10.5194/acp-24-13065-2024, 2024.
- 598 Cai, Y., Ye, C., Chen, W., Hu, W., Song, W., Peng, Y., Huang, S., Qi, J., Wang, S., Wang, C., Wu, C.,  
599 Wang, Z., Wang, B., Huang, X., He, L., Gligorovski, S., Yuan, B., Shao, M., and Wang, X.: The important  
600 contribution of secondary formation and biomass burning to oxidized organic nitrogen (OON) in a  
601 polluted urban area: insights from in situ measurements of a chemical ionization mass spectrometer  
602 (CIMS), *Atmos. Chem. Phys.*, 23, 8855-8877, 10.5194/acp-23-8855-2023, 2023.
- 603 Chacon-Madrid, H. J. and Donahue, N. M.: Fragmentation vs. functionalization: chemical aging



- 604 and organic aerosol formation, *Atmos. Chem. Phys.*, 11, 10553-10563, 10.5194/acp-11-10553-2011,  
605 2011.
- 606 Charan, S. M., Huang, Y., and Seinfeld, J. H.: Computational Simulation of Secondary Organic  
607 Aerosol Formation in Laboratory Chambers, *Chemical Reviews*, 119, 11912-11944,  
608 10.1021/acs.chemrev.9b00358, 2019.
- 609 Canonaco, F., Crippa, M., Slowik, J. G., Baltensperger, U., and Prévôt, A. S. H.: SoFi, an IGOR-  
610 based interface for the efficient use of the generalized multilinear engine (ME-2) for the source  
611 apportionment: ME-2 application to aerosol mass spectrometer data, *Atmos. Meas. Tech.*, 6, 3649-3661,  
612 10.5194/amt-6-3649-2013, 2013.
- 613 Chen, G., Sosedova, Y., Canonaco, F., Fröhlich, R., Tobler, A., Vlachou, A., Daellenbach, K. R.,  
614 Bozzetti, C., Hueglin, C., Graf, P., Baltensperger, U., Slowik, J. G., El Haddad, I., and Prévôt, A. S. H.:  
615 Time-dependent source apportionment of submicron organic aerosol for a rural site in an alpine valley  
616 using a rolling positive matrix factorisation (PMF) window, *Atmos. Chem. Phys.*, 21, 15081-15101,  
617 10.5194/acp-21-15081-2021, 2021a.
- 618 Chen, W. T., Shao, M., Lu, S. H., Wang, M., Zeng, L. M., Yuan, B., and Liu, Y.: Understanding  
619 primary and secondary sources of ambient carbonyl compounds in Beijing using the PMF model, *Atmos.*  
620 *Chem. Phys.*, 14, 3047-3062, 10.5194/acp-14-3047-2014, 2014.
- 621 Chen, Y., Guo, H., Nah, T., Tanner, D. J., Sullivan, A. P., Takeuchi, M., Gao, Z., Vasilakos, P., Russell,  
622 A. G., Baumann, K., Huey, L. G., Weber, R. J., and Ng, N. L.: Low-Molecular-Weight Carboxylic Acids  
623 in the Southeastern U.S.: Formation, Partitioning, and Implications for Organic Aerosol Aging,  
624 *Environmental Science & Technology*, 55, 6688-6699, 10.1021/acs.est.1c01413, 2021b.
- 625 Decker, Z. C. J., Zarzana, K. J., Coggon, M., Min, K.-E., Pollack, I., Ryerson, T. B., Peischl, J.,  
626 Edwards, P., Dubé, W. P., Markovic, M. Z., Roberts, J. M., Veres, P. R., Graus, M., Warneke, C., de Gouw,  
627 J., Hatch, L. E., Barsanti, K. C., and Brown, S. S.: Nighttime Chemical Transformation in Biomass  
628 Burning Plumes: A Box Model Analysis Initialized with Aircraft Observations, *Environmental Science*  
629 *& Technology*, 53, 2529-2538, 10.1021/acs.est.8b05359, 2019.
- 630 Donahue, N. M., Epstein, S. A., Pandis, S. N., and Robinson, A. L.: A two-dimensional volatility  
631 basis set: 1. organic-aerosol mixing thermodynamics, *Atmos. Chem. Phys.*, 11, 3303-3318, 10.5194/acp-  
632 11-3303-2011, 2011.
- 633 Donahue, N. M., Kroll, J. H., Pandis, S. N., and Robinson, A. L.: A two-dimensional volatility basis  
634 set – Part 2: Diagnostics of organic-aerosol evolution, *Atmos. Chem. Phys.*, 12, 615-634, 10.5194/acp-  
635 12-615-2012, 2012.
- 636 Faxon, C., Hammes, J., Le Breton, M., Pathak, R. K., and Hallquist, M.: Characterization of organic  
637 nitrate constituents of secondary organic aerosol (SOA) from nitrate-radical-initiated oxidation of  
638 limonene using high-resolution chemical ionization mass spectrometry, *Atmos. Chem. Phys.*, 18, 5467-  
639 5481, 10.5194/acp-18-5467-2018, 2018.
- 640 Feng, T., Wang, Y., Hu, W., Zhu, M., Song, W., Chen, W., Sang, Y., Fang, Z., Deng, W., Fang, H.,  
641 Yu, X., Wu, C., Yuan, B., Huang, S., Shao, M., Huang, X., He, L., Lee, Y. R., Huey, L. G., Canonaco, F.,  
642 Prevot, A. S. H., and Wang, X.: Impact of aging on the sources, volatility, and viscosity of organic  
643 aerosols in Chinese outflows, *Atmos. Chem. Phys.*, 23, 611-636, 10.5194/acp-23-611-2023, 2023.
- 644 Fisher, J. A., Jacob, D. J., Travis, K. R., Kim, P. S., Marais, E. A., Chan Miller, C., Yu, K., Zhu, L.,  
645 Yantosca, R. M., Sulprizio, M. P., Mao, J., Wennberg, P. O., Crounse, J. D., Teng, A. P., Nguyen, T. B.,  
646 St. Clair, J. M., Cohen, R. C., Romer, P., Nault, B. A., Wooldridge, P. J., Jimenez, J. L., Campuzano-Jost,  
647 P., Day, D. A., Hu, W., Shepson, P. B., Xiong, F., Blake, D. R., Goldstein, A. H., Misztal, P. K., Hanisco,



- 648 T. F., Wolfe, G. M., Ryerson, T. B., Wisthaler, A., and Mikoviny, T.: Organic nitrate chemistry and its  
649 implications for nitrogen budgets in an isoprene- and monoterpene-rich atmosphere: constraints from  
650 aircraft (SEAC4RS) and ground-based (SOAS) observations in the Southeast US, *Atmos. Chem. Phys.*,  
651 16, 5969-5991, 10.5194/acp-16-5969-2016, 2016.
- 652 Gaston, C. J., Lopez-Hilfiker, F. D., Whybrew, L. E., Hadley, O., McNair, F., Gao, H., Jaffe, D. A.,  
653 and Thornton, J. A.: Online molecular characterization of fine particulate matter in Port Angeles, WA:  
654 Evidence for a major impact from residential wood smoke, *Atmospheric Environment*, 138, 99-107,  
655 <https://doi.org/10.1016/j.atmosenv.2016.05.013>, 2016.
- 656 Graham, E. L., Wu, C., Bell, D. M., Bertrand, A., Haslett, S. L., Baltensperger, U., El Haddad, I.,  
657 Krejci, R., Riipinen, I., and Mohr, C.: Volatility of aerosol particles from NO<sub>3</sub> oxidation of various  
658 biogenic organic precursors, *Atmos. Chem. Phys.*, 23, 7347-7362, 10.5194/acp-23-7347-2023, 2023.
- 659 Guo, J., Zhou, S., Cai, M., Zhao, J., Song, W., Zhao, W., Hu, W., Sun, Y., He, Y., Yang, C., Xu, X.,  
660 Zhang, Z., Cheng, P., Fan, Q., Hang, J., Fan, S., Wang, X., and Wang, X.: Characterization of submicron  
661 particles by time-of-flight aerosol chemical speciation monitor (ToF-ACSM) during wintertime: aerosol  
662 composition, sources, and chemical processes in Guangzhou, China, *Atmos. Chem. Phys.*, 20, 7595-7615,  
663 10.5194/acp-20-7595-2020, 2020.
- 664 Hildebrandt Ruiz, L., Paciga, A. L., Cerully, K. M., Nenes, A., Donahue, N. M., and Pandis, S. N.:  
665 Formation and aging of secondary organic aerosol from toluene: changes in chemical composition,  
666 volatility, and hygroscopicity, *Atmos. Chem. Phys.*, 15, 8301-8313, 10.5194/acp-15-8301-2015, 2015.
- 667 Huang, R.-J., Zhang, Y., Bozzetti, C., Ho, K.-F., Cao, J.-J., Han, Y., Daellenbach, K. R., Slowik, J.  
668 G., Platt, S. M., Canonaco, F., Zotter, P., Wolf, R., Pieber, S. M., Bruns, E. A., Crippa, M., Ciarelli, G.,  
669 Piazzalunga, A., Schwikowski, M., Abbaszade, G., Schnelle-Kreis, J., Zimmermann, R., An, Z., Szidat,  
670 S., Baltensperger, U., Haddad, I. E., and Prevot, A. S. H.: High secondary aerosol contribution to  
671 particulate pollution during haze events in China, *Nature*, 514, 218-222, 10.1038/nature13774  
672 [http://www.nature.com/nature/journal/vaop/ncurrent/abs/nature13774.html#supplementary-](http://www.nature.com/nature/journal/vaop/ncurrent/abs/nature13774.html#supplementary-information)  
673 [information](http://www.nature.com/nature/journal/vaop/ncurrent/abs/nature13774.html#supplementary-information), 2014.
- 674 Huang, S., Wu, Z., Poulain, L., van Pinxteren, M., Merkel, M., Assmann, D., Herrmann, H., and  
675 Wiedensohler, A.: Source apportionment of the organic aerosol over the Atlantic Ocean from  
676 53°&thinsp;N to 53°&thinsp;S: significant contributions from marine emissions and long-range transport,  
677 *Atmos. Chem. Phys.*, 18, 18043-18062, 10.5194/acp-18-18043-2018, 2018.
- 678 Huang, W., Saathoff, H., Shen, X., Ramisetty, R., Leisner, T., and Mohr, C.: Seasonal characteristics  
679 of organic aerosol chemical composition and volatility in Stuttgart, Germany, *Atmos. Chem. Phys.*, 19,  
680 11687-11700, 10.5194/acp-19-11687-2019, 2019.
- 681 Huang, X. F., He, L. Y., Hu, M., Canagaratna, M. R., Sun, Y., Zhang, Q., Zhu, T., Xue, L., Zeng, L.  
682 W., Liu, X. G., Zhang, Y. H., Jayne, J. T., Ng, N. L., and Worsnop, D. R.: Highly time-resolved chemical  
683 characterization of atmospheric submicron particles during 2008 Beijing Olympic Games using an  
684 Aerodyne High-Resolution Aerosol Mass Spectrometer, *Atmos. Chem. Phys.*, 10, 8933-8945,  
685 10.5194/acp-10-8933-2010, 2010.
- 686 Iyer, S., Lopez-Hilfiker, F., Lee, B. H., Thornton, J. A., and Kurtén, T.: Modeling the Detection of  
687 Organic and Inorganic Compounds Using Iodide-Based Chemical Ionization, *The Journal of Physical*  
688 *Chemistry A*, 120, 576-587, 10.1021/acs.jpca.5b09837, 2016.
- 689 Jenkin, M. E.: Modelling the formation and composition of secondary organic aerosol from  $\alpha$ - and  
690  $\beta$ -pinene ozonolysis using MCM v3, *Atmos. Chem. Phys.*, 4, 1741-1757, 10.5194/acp-4-1741-2004,  
691 2004.



- Jimenez, J. L., Canagaratna, M., Donahue, N., Prevot, A., Zhang, Q., Kroll, J. H., DeCarlo, P. F., Allan, J. D., Coe, H., and Ng, N. J. S.: Evolution of organic aerosols in the atmosphere, 326, 1525-1529, 2009.
- Jorga, S. D., Florou, K., Kaltsonoudis, C., Kodros, J. K., Vasilakopoulou, C., Cirtog, M., Fouqueau, A., Picquet-Varrault, B., Nenes, A., and Pandis, S. N.: Nighttime chemistry of biomass burning emissions in urban areas: A dual mobile chamber study, *Atmos. Chem. Phys.*, 21, 15337-15349, 10.5194/acp-21-15337-2021, 2021.
- Kroll, J. H. and Seinfeld, J. H.: Chemistry of secondary organic aerosol: Formation and evolution of low-volatility organics in the atmosphere, *Atmospheric Environment*, 42, 3593-3624, <https://doi.org/10.1016/j.atmosenv.2008.01.003>, 2008.
- Kuang, Y., Huang, S., Xue, B., Luo, B., Song, Q., Chen, W., Hu, W., Li, W., Zhao, P., Cai, M., Peng, Y., Qi, J., Li, T., Wang, S., Chen, D., Yue, D., Yuan, B., and Shao, M.: Contrasting effects of secondary organic aerosol formations on organic aerosol hygroscopicity, *Atmos. Chem. Phys.*, 21, 10375-10391, 10.5194/acp-21-10375-2021, 2021.
- Lee, B. P., Li, Y. J., Yu, J. Z., Louie, P. K., and Chan, C. K.: Characteristics of submicron particulate matter at the urban roadside in downtown Hong Kong—Overview of 4 months of continuous high-resolution aerosol mass spectrometer measurements, *Journal of Geophysical Research: Atmospheres*, 120, 7040-7058, 2015.
- Lopez-Hilfiker, F. D., Iyer, S., Mohr, C., Lee, B. H., D'Ambro, E. L., Kurtén, T., and Thornton, J. A.: Constraining the sensitivity of iodide adduct chemical ionization mass spectrometry to multifunctional organic molecules using the collision limit and thermodynamic stability of iodide ion adducts, *Atmos. Meas. Tech.*, 9, 1505-1512, 10.5194/amt-9-1505-2016, 2016.
- Lopez-Hilfiker, F. D., Mohr, C., Ehn, M., Rubach, F., Kleist, E., Wildt, J., Mentel, T. F., Lutz, A., Hallquist, M., Worsnop, D., and Thornton, J. A.: A novel method for online analysis of gas and particle composition: description and evaluation of a Filter Inlet for Gases and AEROsols (FIGAERO), *Atmos. Meas. Tech.*, 7, 983-1001, 10.5194/amt-7-983-2014, 2014.
- Louvaris, E. E., Florou, K., Karnezi, E., Papanastasiou, D. K., Gkatzelis, G. I., and Pandis, S. N.: Volatility of source apportioned wintertime organic aerosol in the city of Athens, *Atmospheric Environment*, 158, 138-147, <https://doi.org/10.1016/j.atmosenv.2017.03.042>, 2017.
- Lu, Q., Murphy, B. N., Qin, M., Adams, P. J., Zhao, Y., Pye, H. O. T., Efstathiou, C., Allen, C., and Robinson, A. L.: Simulation of organic aerosol formation during the CalNex study: updated mobile emissions and secondary organic aerosol parameterization for intermediate-volatility organic compounds, *Atmos. Chem. Phys.*, 20, 4313-4332, 10.5194/acp-20-4313-2020, 2020.
- Matsui, H., Koike, M., Takegawa, N., Kondo, Y., Griffin, R. J., Miyazaki, Y., Yokouchi, Y., and Ohara, T.: Secondary organic aerosol formation in urban air: Temporal variations and possible contributions from unidentified hydrocarbons, *Journal of Geophysical Research: Atmospheres*, 114, <https://doi.org/10.1029/2008JD010164>, 2009.
- Nie, W., Yan, C., Huang, D. D., Wang, Z., Liu, Y., Qiao, X., Guo, Y., Tian, L., Zheng, P., Xu, Z., Li, Y., Xu, Z., Qi, X., Sun, P., Wang, J., Zheng, F., Li, X., Yin, R., Dallenbach, K. R., Bianchi, F., Petäjä, T., Zhang, Y., Wang, M., Schervish, M., Wang, S., Qiao, L., Wang, Q., Zhou, M., Wang, H., Yu, C., Yao, D., Guo, H., Ye, P., Lee, S., Li, Y. J., Liu, Y., Chi, X., Kerminen, V.-M., Ehn, M., Donahue, N. M., Wang, T., Huang, C., Kulmala, M., Worsnop, D., Jiang, J., and Ding, A.: Secondary organic aerosol formed by condensing anthropogenic vapours over China's megacities, *Nature Geoscience*, 15, 255-261, 10.1038/s41561-022-00922-5, 2022.





- Nie, W., Yan, C., Yang, L., Roldin, P., Liu, Y., Vogel, A. L., Molteni, U., Stolzenburg, D., Finkenzeller, H., Amorim, A., Bianchi, F., Curtius, J., Dada, L., Draper, D. C., Duplissy, J., Hansel, A., He, X.-C., Hofbauer, V., Jokinen, T., Kim, C., Lehtipalo, K., Nichman, L., Mauldin, R. L., Makhmutov, V., Mentler, B., Mizelli-Ojdanic, A., Petäjä, T., Quéléver, L. L. J., Schallhart, S., Simon, M., Tauber, C., Tomé, A., Volkamer, R., Wagner, A. C., Wagner, R., Wang, M., Ye, P., Li, H., Huang, W., Qi, X., Lou, S., Liu, T., Chi, X., Dommen, J., Baltensperger, U., El Haddad, I., Kirkby, J., Worsnop, D., Kulmala, M., Donahue, N. M., Ehn, M., and Ding, A.: NO at low concentration can enhance the formation of highly oxygenated biogenic molecules in the atmosphere, *Nature Communications*, 14, 3347, 10.1038/s41467-023-39066-4, 2023.
- Nihill, K. J., Ye, Q., Majluf, F., Krechmer, J. E., Canagaratna, M. R., and Kroll, J. H.: Influence of the NO/NO<sub>2</sub> Ratio on Oxidation Product Distributions under High-NO Conditions, *Environmental Science & Technology*, 55, 6594-6601, 10.1021/acs.est.0c07621, 2021.
- Ou, H. J., Cai, M. F., Liang, B. L., Sun, Q. B., Zhou, S. Z., Xu, Y. S., Ren, L. H., and Zhao, J.: Characterization, Sources, and Chemical Processes of Submicron Aerosols at a Mountain Site in Central China, *Journal of Geophysical Research: Atmospheres*, 128, e2022JD038258, <https://doi.org/10.1029/2022JD038258>, 2023.
- Paatero, P. and Tapper, U.: Positive matrix factorization: A non-negative factor model with optimal utilization of error estimates of data values, *Environmetrics*, 5, 111-126, <https://doi.org/10.1002/env.3170050203>, 1994.
- Paulot, F., Crounse, J. D., Kjaergaard, H. G., Kroll, J. H., Seinfeld, J. H., and Wennberg, P. O.: Isoprene photooxidation: new insights into the production of acids and organic nitrates, *Atmos. Chem. Phys.*, 9, 1479-1501, 10.5194/acp-9-1479-2009, 2009.
- Praske, E., Otkjær, R. V., Crounse, J. D., Hethcox, J. C., Stoltz, B. M., Kjaergaard, H. G., and Wennberg, P. O.: Atmospheric autoxidation is increasingly important in urban and suburban North America, *Proceedings of the National Academy of Sciences*, 115, 64-69, 10.1073/pnas.1715540115, 2018.
- Pye, H. O. T., D'Ambro, E. L., Lee, B. H., Schobesberger, S., Takeuchi, M., Zhao, Y., Lopez-Hilfiker, F., Liu, J., Shilling, J. E., Xing, J., Mathur, R., Middlebrook, A. M., Liao, J., Welti, A., Graus, M., Warneke, C., de Gouw, J. A., Holloway, J. S., Ryerson, T. B., Pollack, I. B., and Thornton, J. A.: Anthropogenic enhancements to production of highly oxygenated molecules from autoxidation, *Proceedings of the National Academy of Sciences*, 116, 6641-6646, 10.1073/pnas.1810774116, 2019.
- Qin, Y. M., Tan, H. B., Li, Y. J., Schurman, M. I., Li, F., Canonaco, F., Prévôt, A. S. H., and Chan, C. K.: The role of traffic emissions in particulate organics and nitrate at a downwind site in the periphery of Guangzhou, China, *Atmospheric Chemistry & Physics*, 1-31, 2017.
- Ren, S., Yao, L., Wang, Y., Yang, G., Liu, Y., Li, Y., Lu, Y., Wang, L., and Wang, L.: Volatility parameterization of ambient organic aerosols at a rural site of the North China Plain, *Atmos. Chem. Phys.*, 22, 9283-9297, 10.5194/acp-22-9283-2022, 2022.
- Rissanen, M. P.: NO<sub>2</sub> Suppression of Autoxidation–Inhibition of Gas-Phase Highly Oxidized Dimer Product Formation, *ACS Earth and Space Chemistry*, 2, 1211-1219, 10.1021/acsearthspacechem.8b00123, 2018.
- Rudich, Y., Donahue, N. M., and Mentel, T. F.: Aging of Organic Aerosol: Bridging the Gap Between Laboratory and Field Studies, *Annual Review of Physical Chemistry*, 58, 321-352, <https://doi.org/10.1146/annurev.physchem.58.032806.104432>, 2007.
- Shrivastava, M., Andreae, M. O., Artaxo, P., Barbosa, H. M. J., Berg, L. K., Brito, J., Ching, J.,



- 780 Easter, R. C., Fan, J., Fast, J. D., Feng, Z., Fuentes, J. D., Glasius, M., Goldstein, A. H., Alves, E. G.,  
781 Gomes, H., Gu, D., Guenther, A., Jathar, S. H., Kim, S., Liu, Y., Lou, S., Martin, S. T., McNeill, V. F.,  
782 Medeiros, A., de Sá, S. S., Shilling, J. E., Springston, S. R., Souza, R. A. F., Thornton, J. A., Isaacman-  
783 VanWertz, G., Yee, L. D., Ynoue, R., Zaveri, R. A., Zelenyuk, A., and Zhao, C.: Urban pollution greatly  
784 enhances formation of natural aerosols over the Amazon rainforest, *Nature Communications*, 10, 1046,  
785 10.1038/s41467-019-08909-4, 2019.
- 786 Thornton, J. A., Mohr, C., Schobesberger, S., D'Ambro, E. L., Lee, B. H., and Lopez-Hilfiker, F. D.:  
787 Evaluating Organic Aerosol Sources and Evolution with a Combined Molecular Composition and  
788 Volatility Framework Using the Filter Inlet for Gases and Aerosols (FIGAERO), *Accounts of Chemical*  
789 *Research*, 53, 1415-1426, 10.1021/acs.accounts.0c00259, 2020.
- 790 Tian, S. L., Pan, Y. P., and Wang, Y. S.: Size-resolved source apportionment of particulate matter in  
791 urban Beijing during haze and non-haze episodes, *Atmos. Chem. Phys.*, 16, 1-19, 10.5194/acp-16-1-2016,  
792 2016.
- 793 Ulbrich, I. M., Canagaratna, M. R., Zhang, Q., Worsnop, D. R., and Jimenez, J. L.: Interpretation of  
794 organic components from Positive Matrix Factorization of aerosol mass spectrometric data, *Atmos.*  
795 *Chem. Phys.*, 9, 2891-2918, 10.5194/acp-9-2891-2009, 2009.
- 796 Walser, M. L., Park, J., Gomez, A. L., Russell, A. R., and Nizkorodov, S. A.: Photochemical Aging  
797 of Secondary Organic Aerosol Particles Generated from the Oxidation of d-Limonene, *The Journal of*  
798 *Physical Chemistry A*, 111, 1907-1913, 10.1021/jp066293l, 2007.
- 799 Wang, Y., Clusius, P., Yan, C., Dällenbach, K., Yin, R., Wang, M., He, X.-C., Chu, B., Lu, Y., Dada,  
800 L., Kangasluoma, J., Rantala, P., Deng, C., Lin, Z., Wang, W., Yao, L., Fan, X., Du, W., Cai, J., Heikkinen,  
801 L., Tham, Y. J., Zha, Q., Ling, Z., Junninen, H., Petäjä, T., Ge, M., Wang, Y., He, H., Worsnop, D. R.,  
802 Kerminen, V.-M., Bianchi, F., Wang, L., Jiang, J., Liu, Y., Boy, M., Ehn, M., Donahue, N. M., and  
803 Kulmala, M.: Molecular Composition of Oxygenated Organic Molecules and Their Contributions to  
804 Organic Aerosol in Beijing, *Environmental Science & Technology*, 56, 770-778,  
805 10.1021/acs.est.1c05191, 2022.
- 806 Ulbrich, I. M., Canagaratna, M. R., Zhang, Q., Worsnop, D. R., and Jimenez, J. L.: Interpretation of  
807 organic components from Positive Matrix Factorization of aerosol mass spectrometric data, *Atmos.*  
808 *Chem. Phys.*, 9, 2891-2918, 10.5194/acp-9-2891-2009, 2009.
- 809 Uchida, K., Ide, Y., and Takegawa, N.: Ionization efficiency of evolved gas molecules from aerosol  
810 particles in a thermal desorption aerosol mass spectrometer: Laboratory experiments, *Aerosol Sci Tech*,  
811 53, 86-93, 10.1080/02786826.2018.1544704, 2019.
- 812 Wu, C., Bell, D. M., Graham, E. L., Haslett, S., Riipinen, I., Baltensperger, U., Bertrand, A.,  
813 Giannoukos, S., Schoonbaert, J., El Haddad, I., Prevot, A. S. H., Huang, W., and Mohr, C.: Photolytically  
814 induced changes in composition and volatility of biogenic secondary organic aerosol from nitrate radical  
815 oxidation during night-to-day transition, *Atmos. Chem. Phys.*, 21, 14907-14925, 10.5194/acp-21-14907-  
816 2021, 2021.
- 817 Xu, W., Chen, C., Qiu, Y., Li, Y., Zhang, Z., Karnezi, E., Pandis, S. N., Xie, C., Li, Z., Sun, J., Ma,  
818 N., Xu, W., Fu, P., Wang, Z., Zhu, J., Worsnop, D. R., Ng, N. L., and Sun, Y.: Organic aerosol volatility  
819 and viscosity in the North China Plain: contrast between summer and winter, *Atmos. Chem. Phys.*, 21,  
820 5463-5476, 10.5194/acp-21-5463-2021, 2021.
- 821 Xu, X., Wang, G., Gao, Y., Zhang, S., Chen, L., Li, R., Li, Z., and Li, R.: Smog chamber study on  
822 the NO<sub>x</sub> dependence of SOA from isoprene photo-oxidation: implication on RO<sub>2</sub> chemistry, *Journal of*  
823 *Environmental Sciences*, <https://doi.org/10.1016/j.jes.2025.05.024>, 2025.



824 Yang, S., Yuan, B., Peng, Y., Huang, S., Chen, W., Hu, W., Pei, C., Zhou, J., Parrish, D. D., Wang,  
825 W., He, X., Cheng, C., Li, X. B., Yang, X., Song, Y., Wang, H., Qi, J., Wang, B., Wang, C., Wang, C.,  
826 Wang, Z., Li, T., Zheng, E., Wang, S., Wu, C., Cai, M., Ye, C., Song, W., Cheng, P., Chen, D., Wang, X.,  
827 Zhang, Z., Wang, X., Zheng, J., and Shao, M.: The formation and mitigation of nitrate pollution:  
828 comparison between urban and suburban environments, *Atmos. Chem. Phys.*, 22, 4539-4556,  
829 10.5194/acp-22-4539-2022, 2022.

830 Ye, C., Liu, Y., Yuan, B., Wang, Z., Lin, Y., Hu, W., Chen, W., Li, T., Song, W., Wang, X., Lv, D.,  
831 Gu, D., and Shao, M.: Low-NO-like Oxidation Pathway Makes a Significant Contribution to Secondary  
832 Organic Aerosol in Polluted Urban Air, *Environmental Science & Technology*, 10.1021/acs.est.3c01055,  
833 2023.

834 Ye, C., Yuan, B., Lin, Y., Wang, Z., Hu, W., Li, T., Chen, W., Wu, C., Wang, C., Huang, S., Qi, J.,  
835 Wang, B., Wang, C., Song, W., Wang, X., Zheng, E., Krechmer, J. E., Ye, P., Zhang, Z., Wang, X.,  
836 Worsnop, D. R., and Shao, M.: Chemical characterization of oxygenated organic compounds in the gas  
837 phase and particle phase using iodide CIMS with FIGAERO in urban air, *Atmos. Chem. Phys.*, 21, 8455-  
838 8478, 10.5194/acp-21-8455-2021, 2021.

839 Zhang, Q., Jimenez, J. L., Canagaratna, M. R., Ulbrich, I. M., Ng, N. L., Worsnop, D. R., and Sun,  
840 Y.: Understanding atmospheric organic aerosols via factor analysis of aerosol mass spectrometry: a  
841 review, *Analytical and Bioanalytical Chemistry*, 401, 3045-3067, 10.1007/s00216-011-5355-y, 2011.

842 Zhang, Y. L., El-Haddad, I., Huang, R. J., Ho, K. F., Cao, J. J., Han, Y., Zotter, P., Bozzetti, C.,  
843 Daellenbach, K. R., Slowik, J. G., Salazar, G., Prévôt, A. S. H., and Szidat, S.: Large contribution of  
844 fossil fuel derived secondary organic carbon to water soluble organic aerosols in winter haze in China,  
845 *Atmos. Chem. Phys.*, 18, 4005-4017, 10.5194/acp-18-4005-2018, 2018.

846 Zhao, W., Kawamura, K., Yue, S., Wei, L., Ren, H., Yan, Y., Kang, M., Li, L., Ren, L., Lai, S., Li,  
847 J., Sun, Y., Wang, Z., and Fu, P.: Molecular distribution and compound-specific stable carbon isotopic  
848 composition of dicarboxylic acids, oxocarboxylic acids and  $\alpha$ -dicarbonyls in PM<sub>2.5</sub> from Beijing, China,  
849 *Atmos. Chem. Phys.*, 18, 2749-2767, 10.5194/acp-18-2749-2018, 2018.

850 Zheng, Y., Chen, Q., Cheng, X., Mohr, C., Cai, J., Huang, W., Shrivastava, M., Ye, P., Fu, P., Shi,  
851 X., Ge, Y., Liao, K., Miao, R., Qiu, X., Koenig, T. K., and Chen, S.: Precursors and Pathways Leading to  
852 Enhanced Secondary Organic Aerosol Formation during Severe Haze Episodes, *Environmental Science*  
853 *& Technology*, 10.1021/acs.est.1c04255, 2021.

854 Zhou, W., Xu, W., Kim, H., Zhang, Q., Fu, P., Worsnop, D. R., and Sun, Y.: A review of aerosol  
855 chemistry in Asia: insights from aerosol mass spectrometer measurements, *Environmental Science:*  
856 *Processes & Impacts*, 22, 1616-1653, 10.1039/D0EM00212G, 2020.

857

858



**Table 1.** The average volatility ( $\log_{10} \overline{C^*}$ ),  $T_{max}$ , signal-weighted average values of elemental composition, carbon oxidation state ( $\overline{OS_c}$ ), H:C, O:C, N:C for all FIGAERO-OA factors. The estimation of  $\overline{OS_c}$  can be found in Section S2. The volatility of each FIGAERO-OA factor was estimated based on their corresponding  $T_{max}$  using eq. (8) and (9).

	$\log_{10} \overline{C^*}$ ( $\mu\text{g m}^{-3}$ )	$T_{max}$ ( $^{\circ}\text{C}$ )	Composition	$\overline{OS_c}$	H:C	O:C	N:C
Day-HNO <sub>x</sub> -LVOA	-0.98	84.52	C <sub>7.37</sub> H <sub>10.51</sub> O <sub>4.99</sub> N <sub>0.36</sub>	-0.01	1.37	0.75	0.06
Day-LNO <sub>x</sub> -LVOA	-2.71	103.29	C <sub>6.52</sub> H <sub>8.77</sub> O <sub>4.54</sub> N <sub>0.22</sub>	0.18	1.35	0.80	0.04
Day-aged-LVOA	-2.02	95.53	C <sub>6.35</sub> H <sub>8.75</sub> O <sub>5.13</sub> N <sub>0.21</sub>	0.35	1.42	0.91	0.04
Day-aged-ELVOA	-4.80	126.65	C <sub>5.22</sub> H <sub>7.36</sub> O <sub>4.20</sub> N <sub>0.16</sub>	0.40	1.55	1.00	0.03
Day-urban-LVOA	-0.90	83.03	C <sub>6.50</sub> H <sub>9.27</sub> O <sub>4.71</sub> N <sub>0.24</sub>	0.08	1.43	0.80	0.04
Day-urban-ELVOA	-7.18	153.22	C <sub>6.57</sub> H <sub>8.54</sub> O <sub>4.61</sub> N <sub>0.24</sub>	0.26	1.35	0.84	0.05
BB-LVOA	-2.36	99.39	C <sub>6.72</sub> H <sub>9.78</sub> O <sub>4.61</sub> N <sub>0.26</sub>	-0.08	1.47	0.74	0.04
Night-LVOA	-2.02	95.53	C <sub>7.69</sub> H <sub>11.04</sub> O <sub>5.19</sub> N <sub>0.47</sub>	-0.09	1.47	0.77	0.07

863

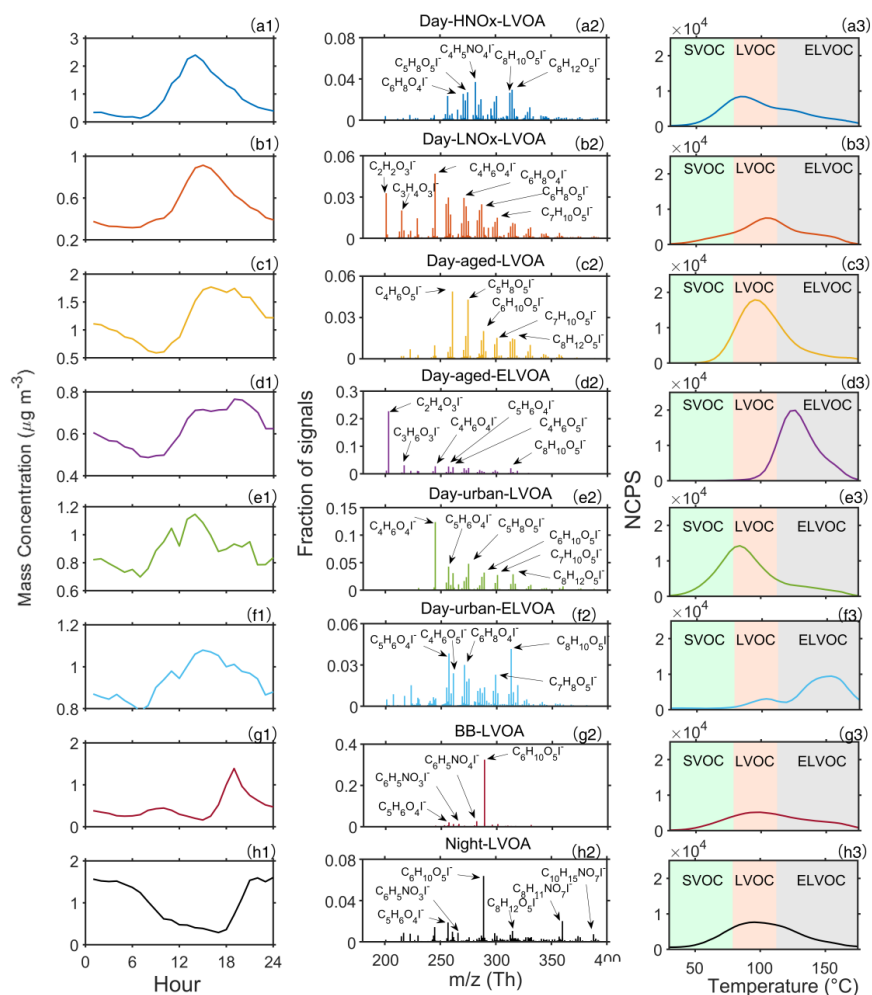
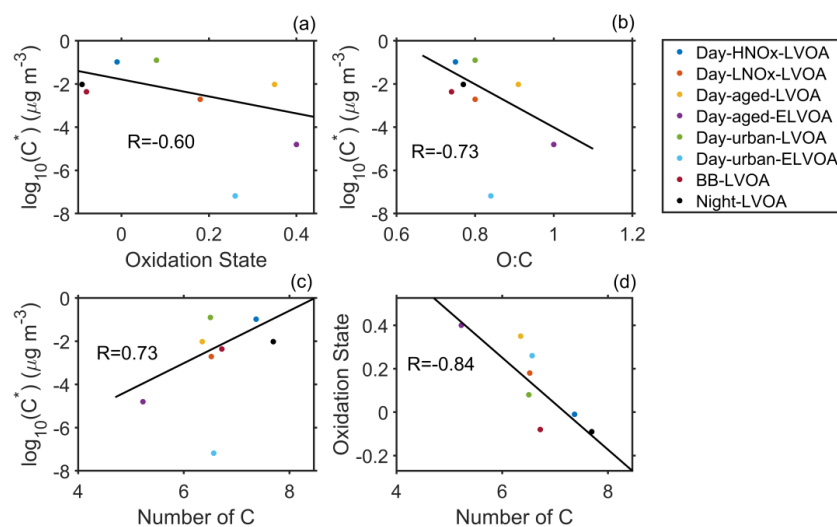


**Figure 1.** Diurnal variation (a1 to h1), mass spectra (a2 to h2), and thermograms (a3 to h3) of FIGAERO-OA factors.



868

869 **Figure 2.** The average volatility of FIGAERO-OA factor vs. (a) oxidation state ( $\overline{OS}_c$ ), (b) O:C ,

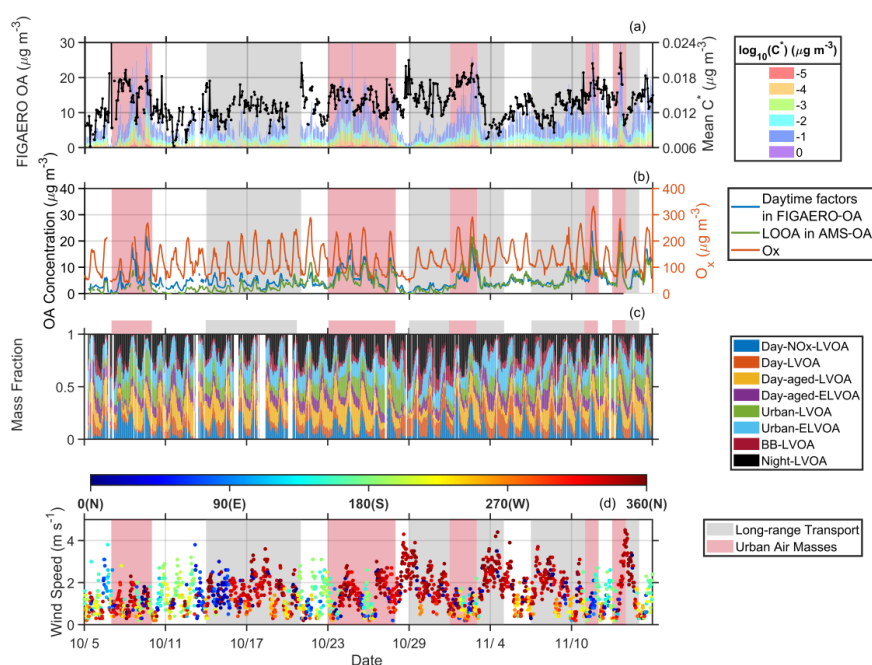
870 and (c) number of carbons and (d) Number of carbons vs.  $\overline{OS}_c$  of thermogram factor. Day-urban-

871 ELVOA is excluded in the estimation of R.

872



873



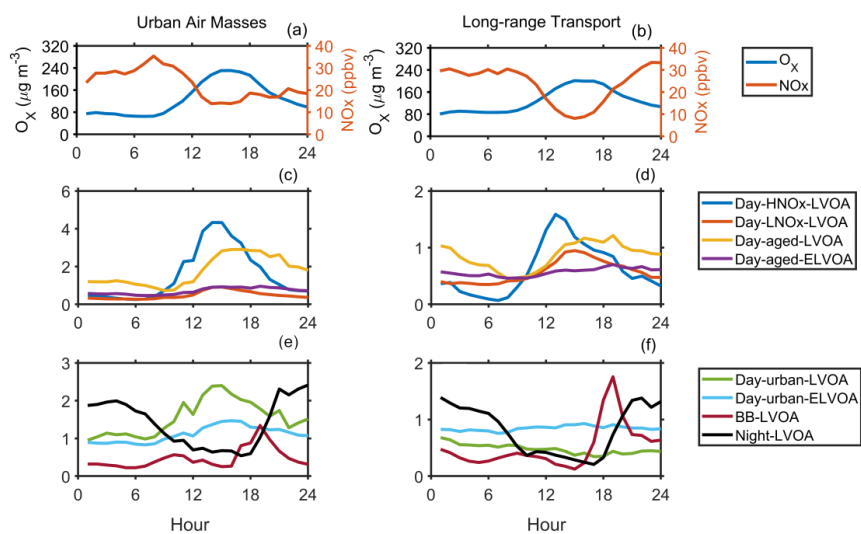
874

875 **Figure 3.** Time series of (a) volatility (presented in a range from  $10^{-5}$  to  $10^0 \mu\text{g m}^{-3}$ ) of FIGAERO-  
876 OA and mean  $C^*$ , (b) daytime factors (Day- $\text{HNO}_x$ -LVOA, Day- $\text{LNO}_x$ -LVOA, Day-aged-LVOA,  
877 Day-aged-ELVOA, Urban LVOA, and Day-urban-ELVOA) in FIGAERO-OA and LOOA factor  
878 from PMF analysis of SP-AMS data, (c) mass fraction of eight FIGAERO-OA factors, and (d) wind  
879 speed and wind direction.

880



881



882

883 **Figure 4.** The average diurnal variation of  $O_3$ ,  $NO_x$ , and mass concentration of eight thermogram

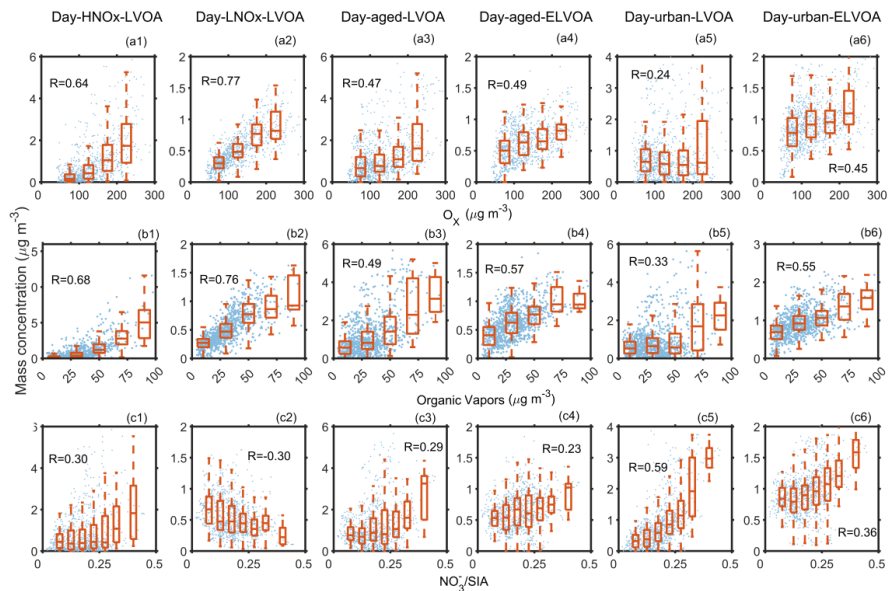
884 factors during the long-range transport (a, c, and e) and urban air masses (b, d, and f) period.

885





886



887

888

889

890

891

892

**Figure 5.** Relationship between the mass concentration of six daytime thermogram factors and (a1-6)  $O_x$ , (b1-6) organic vapors, (c1-6) nitrate fraction in secondary inorganic aerosol (SIA), and (d1-6) sulfate fraction in SIA measured by the FIGAERO-CIMS. The organic vapors are the sum of organic compounds in the gas-phase measured by the FIGAERO-CIMS.

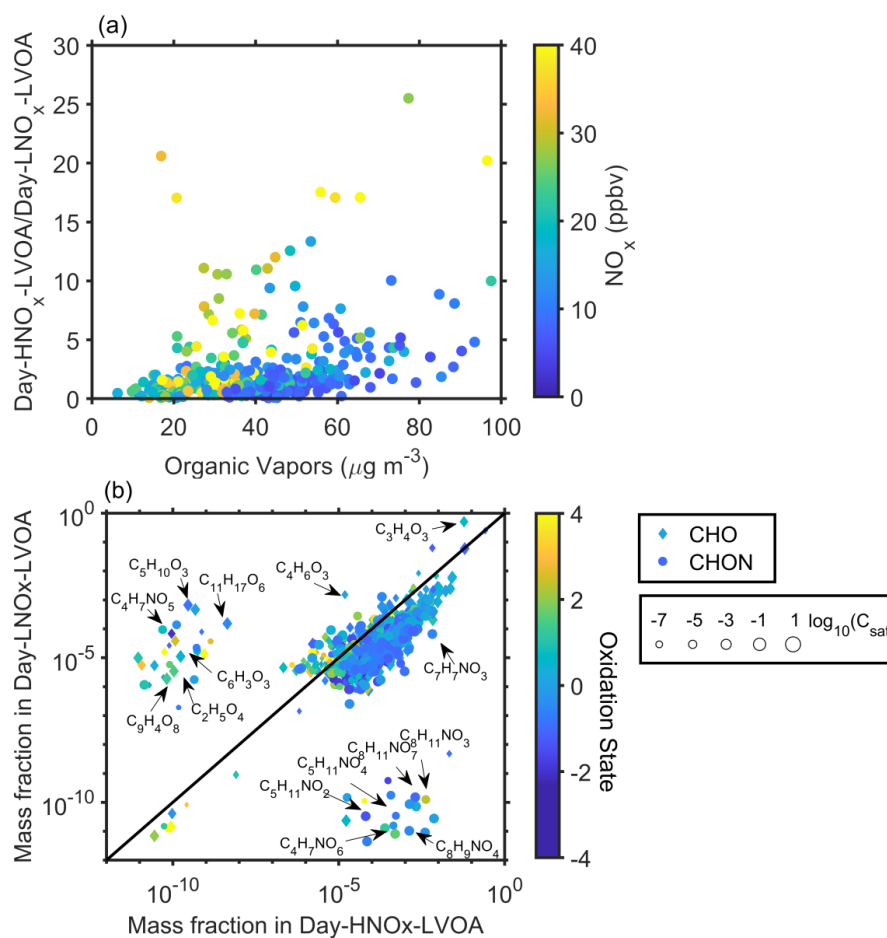
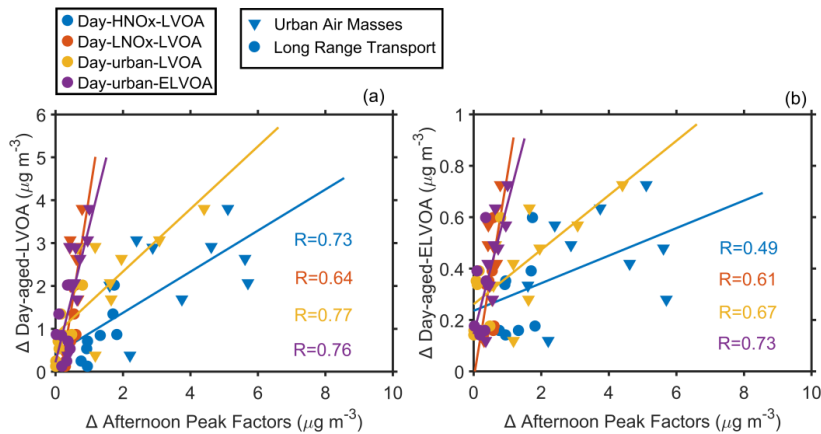


**Figure 6.** (a) Correlation between organic vapors and the ratio of Day-HNO<sub>x</sub>-LVOA to Day-LNO<sub>x</sub>-LVOA. (b) Scatterplots of mass fraction of different species in Day-HNO<sub>x</sub>-LVOA and Day-LNO<sub>x</sub>-LVOA. The color of dots in panel (a) denotes the corresponding NO<sub>x</sub>. The shape, size, and color of markers in panel (b) represents the class of species, volatility, and  $\overline{OS}_C$ , respectively.



899



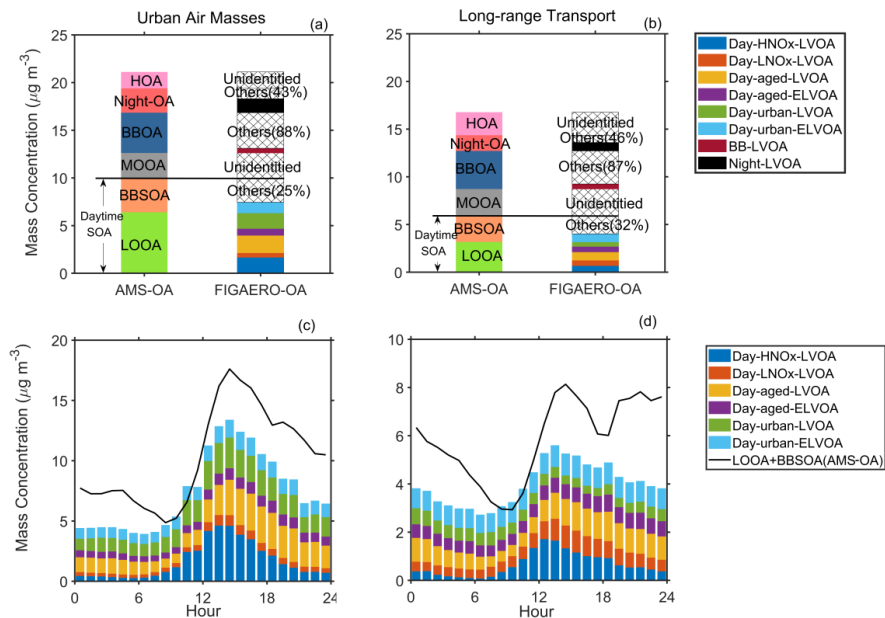
900

901 **Figure 7.** Correlation between the enhancement of (a) Day-aged-LVOA and afternoon peak factors  
902 and (b) Day-aged-ELVOA and afternoon peak factors. Afternoon peak factors include Day-HNO<sub>x</sub>-  
903 LVOA, Day-LNO<sub>x</sub>-LVOA, Day-urban-LVOA, and Day-urban-ELVOA. For afternoon peak factors,  
904 the enhancement ( $\Delta$ ) was regarded as the average mass concentration during 00:00-6:00 LT and  
905 12:00-18:00 LT. For Day-aged-LVOA and Day-aged-ELVOA, the enhancement ( $\Delta$ ) was estimated  
906 as the difference between average mass concentration during 00:00-6:00 LT and 12:00-18:00 LT.

907



908



909

910

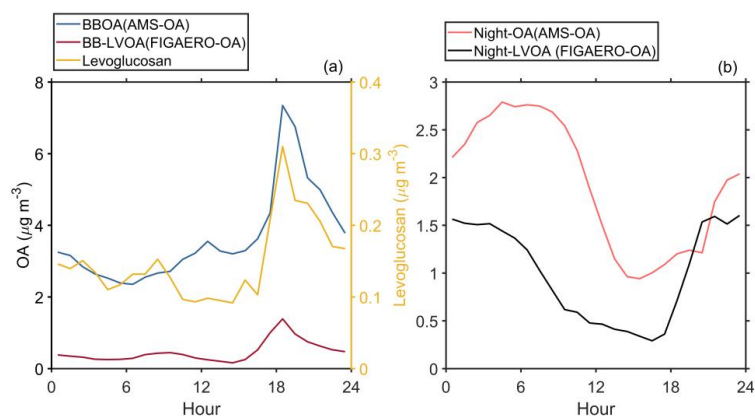
911

912

**Figure 8.** Comparison of the average mass concentration (a and b) and diurnal variation (c and d) of AMS-OA and FIGAERO-OA during long-range transport and urban air masses period.



913



914

915 **Figure 9. (a)** Diurnal variation of BBOA from AMS, BB-LVOA and levoglucosan from FIGAERO-

916 CIMS; (b) Diurnal variation of Night-OA from AMS, and Night-LVOA from FIGAERO-CIMS.

917